1970

The preparation and some high temperature properties of the rare earth trifluorides

David Courtland Henderson
Iowa State University

THE PREPARATION AND SOME HIGH TEMPERATURE PROPERTIES OF THE RARE EARTH TRIFLUORIDES

by

David Courtland Henderson

A Dissertation Submitted to the
Graduate Faculty in Partial Fulfillment of
The Requirements for the Degree of
DOCTOR OF PHILOSOPHY

Major Subject: Physical Chemistry

Approved:

Signature was redacted for privacy.

In Charge of Major Work

Signature was redacted for privacy.

Head of Major Department

Signature was redacted for privacy.

Dean of Graduate College

Iowa State University
Of Science and Technology
Ames, Iowa

1970

TABLE OF CONTENTS

INTRODUCTION

The true rare earths are the elements in the periodic table between elements 58 and 71, inclusive. These are the elements that balance the increasing charge on the nucleus by adding electrons to the inner 4f subshell. Since this subshell can only contain fourteen electrons, there are only fourteen true rare earths. However, the group IIIA elements scandium, yttrium and lanthanum are usually included when describing the rare earths. Yttrium, scandium and lanthanum have three valence electrons giving them physical and chemical properties similar to the rare earths. In addition, these group IIIA elements usually occur in nature with the true rare earths.

The first of the rare earths were discovered in the late 1700's, but it was not until recently that they have become available in high purity in reasonable quantities. Because of this, accurate data on the physical and chemical properties of the rare earth elements and their compounds were scarce until recently. Accurate data is still rather incomplete for some compounds and is being updated as new techniques provide higher purity materials and more precise measurement of the properties.

Although the anhydrous rare earth trifluorides were prepared by Moissan at the end of the last century and have been used in recent years to prepare the rare earth metals, it has only been in the last few years that interest in the prepara-

tion and properties of very high purity fluorides has been renewed. In addition to the need for higher purity fluorides to improve the purity of the rare earth metals, several industrial applications for high purity fluorides have sparked this interest. Examples of some areas of industrial interest are

(1) the use of the light rare earth fluorides as laser materials.

(2) the use of single crystal LaF_3 as a possible replacement for several of the optical fluoride systems in use in infrared and ultraviolet equipment.

(3) the use of rare earth fluorides as a host matrix or to dope other matrix materials for use in phosphors for lighting applications.

(4) the use of LaF_3 as a high temperature lubricant in high pressure steam generators.

In the search for new and better materials for practical applications, the engineer, physicist, or chemist many times needs to know the properties of existing materials. Towards this end, basic physical properties such as crystal structures, transition temperatures, melting points and other similar properties are minimal requirements. In addition, knowledge of the thermodynamic properties, the relationships between temperature, pressure, energy and related quantities can allow the scientist to predict chemical behavior.

Although thermodynamic properties can be estimated from theory for gaseous materials with reasonable accuracy, this is

not generally true for solids. The most reliable thermodynamic data for solids at high temperatures comes from experimental data. These experimental data are usually obtained by the use of calorimetric techniques which yield data in the form of either heat contents or heat capacities.

The heat capacity of a material is defined by the expression dQ/dT, where the amount of heat added to the system, dQ, causes a corresponding rise in the temperature of the system dT. The heat capacity is mathematically undefined unless the independent variables are specified under the conditions of the temperature rise. The heat capacities of particular importance are those at constant volume and at constant pressure.

The heat capacity at constant volume, C_v, is of particular interest from a theoretical point of view as it is directly related to the internal energy, E, of the system from the definition

$$C_v = \left(\frac{dQ}{dT}\right)_V = \left(\frac{\partial E}{\partial T}\right)_V \qquad (1)$$

The heat capacity at constant volume is very difficult to obtain experimentally. It is much easier to obtain the heat capacity at constant pressure which is defined by

$$C_p = \left(\frac{dQ}{dT}\right)_p = \left(\frac{\partial H}{\partial T}\right)_p \qquad (2)$$

where H is the enthalpy or heat content of the system under observation. The other thermodynamic functions can then be calculated from the heat capacity as a function of temperature. The heat content or enthalpy change, ΔH, can be calculated

from the relationship

$$\Delta H = \int C_p dT \tag{3}$$

The entropy change, ΔS, can be calculated from the relationship

$$\Delta S = \int \frac{C_p \, dT}{T} \tag{4}$$

and the free energy change, ΔF, can be calculated from the relationship

$$\Delta F = \Delta H - T\Delta S \tag{5}$$

From the point of view of thermodynamics, the thermodynamic functions can be calculated just as well directly from heat content data. From the First Law of Thermodynamics, the heat content or enthalpy change for a system at constant pressure is given by

$$dH = dQ \tag{6}$$

where dQ can be directly measured with a drop calorimeter. The heat capacity, C_p, can be calculated from the relationship

$$C_p = \left(\frac{\partial(\Delta H)}{\partial T}\right)_P \tag{7}$$

the entropy change, ΔS, can be calculated from the relationship

$$\Delta S = \frac{d(\Delta H)}{T} \tag{8}$$

and the free energy change can be calculated from equation 5.

PART I. THE PREPARATION AND PURIFICATION OF THE ANHYDROUS RARE EARTH TRIFLUORIDES

HISTORICAL

This section has been presented in two parts dealing with (1) the preparation of the anhydrous rare earth fluorides and (2) the purification of the anhydrous rare earth fluorides. The discussion has been limited to only the trifluorides.

The Preparation of the Anhydrous Rare Earth Fluorides

The rare earth trifluorides were first prepared in the laboratory by Moissan (1,2,3) in the 1890's by fluorination of mixtures of rare earth metals or carbides. Since it is easier to directly fluorinate the oxide, Moissan's method now finds little application.

In 1941, Von Wartenburg (4) prepared the fluorides of neodymium and praseodymium by passing a heated stream of hydrogen fluoride (HF) over the oxides. In 1953, Zalkin and Templeton (5) passed a mixture of hydrogen and HF over the rare earth sesquioxides in a platinum apparatus to obtain milligram quantities of rare earth trifluorides for x-ray crystal structure determinations.

However, little work was done on the preparation of anhydrous rare earth fluorides in quantities greater than a few grams until the 1950's, when interest in the pure rare earth metals renewed interest in the fluorides.

Spedding and Daane (6), Carlson and Schmidt (7) and Smutz et al. (8) of this laboratory have reported the preparation of pound quantities of high purity rare earth fluorides using the reaction of anhydrous HF with the oxides.

Spedding and Daane (6) in 1956 reported the preparation of the pure rare earth trifluorides by the reaction of the oxide with ammonium bifluoride. Carlson and Schmidt (7), Walker and Olson (9) and Thoma et al. (10-13) have also prepared yttrium and other rare earth trifluorides with good success using this method.

The thermal dehydration of hydrates of the rare earth fluorides precipitated from an aqueous solution has also been used. The hydrated fluoride was usually precipitated from a solution of the appropriate oxide dissolved in hydrochloric acid (6,14-19). To circumvent the difficulty of obtaining easily filtered precipitates of the hydrates, Daane and Spedding (17) were able to obtain an easily filtered precipitate by digesting the aqueous chloride-HF mixture on a water bath. Popov and Glockler (20) obtained an easily filterable, crystalline precipitate by slow addition of a 40% solution of HF to a solution of rare earth nitrate in 95% ethanol.

Tischer and Burnet (21) have attempted to prepare yttrium fluoride by the action of fluorine gas on the sesquioxide and trichloride. They found that although elevated temperatures and pressures were used, the degree of conversion of the oxide or the chloride to the fluoride was not sufficient to make the

process of interest. The tetravalent fluorides of Ce, Pr, Nd and Tb have been prepared (14,22) by the reaction of fluorine gas with the appropriate trifluoride at elevated temperatures.

Popov and co-workers (20,23) have attempted to prepare the rare earth fluorides using chlorine trifluoride and bromine trifluoride. They reported that bromine trifluoride would not react to any appreciable extent with the oxides. Chlorine trifluoride would react only very slightly with the oxides under anhydrous conditions, even at temperatures of 800°C. However, in the presence of moisture, the rare earth oxides of lanthanum through samarium were almost completely converted to the trifluoride by ClF_3. The oxides of europium through erbium would react with ClF_3 to give yields of 80% for gadolinium to only about 12% for erbium, and the oxides of thulium through lutetium did not react with ClF_3. The reaction of yttrium oxide with ClF_3 gave yields of approximately 45%.

Purification of the Anhydrous Rare Earth Fluorides

The above techniques resulted in an anhydrous fluoride which may contain appreciable amounts of unreacted oxide and oxyfluoride as residual impurities. It has only been within the last five to ten years that attempts to remove these residual impurities have been reported. Interest in the higher purity fluoride materials has been brought about by possible industrial applications requiring highly transparent materials and by the desire to prepare rare earth metals of higher

purity.

Moriarty (24) reduced the oxygen content of the heavy rare earth fluorides for metal reduction by passing HF over a molten salt mixture of rare earth fluoride and LiF, which was used as a fluxing salt. The LiF impurity was not a problem since the fluorides were reduced to the metal with lithium.

Guggenheim (25) reported less opacity in LaF_3 crystals when they were grown in sealed crucibles containing an atmosphere of purified helium and a small partial pressure of HF. The decrease in the opacity was said to be due to a reduction in the oxygen content of the fluoride. Warshaw and Jackson (26) and Robinson and Cripe (27) have also reported less opacity in rare earth fluorides heated to high temperatures in a dynamic HF atmosphere. Muir and Stein (28) have prepared highly transparent LaF_3 crystals by a zone refining technique employing a dynamic HF atmosphere.

METHODS AND GENERAL CONSIDERATIONS

In preparing a high purity material, impurities must either be kept out during preparation or removed from the materials at a later date. Since the rare earths and many of their compounds are excellent getters, it is much easier to try to exclude impurities during preparation than it is to remove them after the materials are prepared. It was, therefore, the intent of this work to convert each rare earth oxide to its respective fluoride in such a way as to introduce the least number of impurities and then to remove or reduce any impurities that might remain.

Of the many techniques which have been used in efforts to prepare pure anhydrous rare earth fluorides, only three appear to merit further consideration at this time:

(1) the reaction of the oxide with anhydrous HF.

(2) the reaction of the oxide with ammonium bifluoride.

(3) the dehydration of the hydrated fluoride obtained by precipitation of the fluoride in aqueous solution with hydrofluoric acid.

The other methods will not be considered here since they have been shown to yield either an impure fluoride or show an unsatisfactory product yield. A brief description of each process and the inherent advantages and disadvantages are discussed below.

The reaction of the rare earth oxide with anhydrous HF

The rare earth fluoride is usually prepared by passing anhydrous HF directly over the oxide at elevated temperatures. The reaction is given by

$$R_2O_3 + 6HF \xrightarrow{700^{\circ}C.} 2RF_3 + 3H_2O \qquad (9)$$

For one or two pound batches, the oxide is placed in a platinum boat which is then placed in a horizontal Inconel tube equiped with inlet and outlet lines for the anhydrous HF and gaseous reaction products. The Inconel tube is then heated to about 700°C. by electrical resistance, and an excess of approximately 200% of HF gas in passed over the oxide during an eight hour period. Carlson and Schmidt (7) have produced LaF_3, CeF_3, NdF_3, SmF_3, EuF_3, TmF_3, YbF_3, LuF_3 and YF_3 by this technique with conversions ranging from 99.90 to 99.98%.

The principle disadvantage of this method comes from the extremely corrosive nature of anhydrous HF at elevated temperatures. If an Inconel tube, as has been used in the past, is used to contain the HF at 700°C., trace impurities of iron, nickel and chromium are likely to be found in the rare earth fluoride. This is due to the fact that Inconel is attacked by HF at temperatures over 600°C. thereby liberating possible volatile fluorides of iron, nickel and chromium which can be picked up by the hot rare earth fluorides. The corrosion problem can be circumvented by the use of materials that are unreactive towards HF.

A second disadvantage arises from the fact that this is a gas-solid reaction. Variables such as the temperature, bed depth and the oxide particle size must be carefully determined and controlled. If these variables are not properly controlled the yield and product quality can be severely affected by the formation of oxyfluorides and/or by the incomplete reaction of the oxide.

The oxyfluoride is formed by the hydrolysis of the rare earth fluoride by water vapor. The hydrolysis reaction is given by

$$RF_3 + H_2O \longrightarrow ROF + 2HF \qquad (10)$$

The oxyfluoride (ROF) is quite stable and can only be converted back to the fluoride with great difficulty.

The reaction of the oxide with ammonium bifluoride

The use of ammonium bifluoride (NH_4HF_2) as a direct hydrofluorinating agent for the preparation of all the rare earth fluorides was developed by Spedding and Daane (6). Up to a kilogram of fluoride can be produced by blending a 30% excess of high purity NH_4HF_2 with the oxide, placing the mixture in a platinum tray inside an Inconel chamber and heating the tube to 300°C. by electrical resistance. A stream of dry air is passed through the chamber to sweep the volatile reaction products and excess NH_4HF_2 from the system. The reaction for converting the oxide to the fluoride by this method is

$$R_2O_3 + 6NH_4HF_2 \xrightarrow{300^\circ C.} 2RF_3 + 6NH_4F + 3H_2O \qquad (11)$$

Although this reaction has the advantages of giving relatively few corrosion problems and employing materials that are easily handled, there are several disadvantages. Ammonium bifluoride obtained commercially usually contains large amounts of iron and calcium. To reduce the iron and calcium content, the ammonium bifluoride is prepared by the reaction of hydrofluoric acid on ammonium carbonate. In addition to adding another step to the process, the specially prepared ammonium bifluoride still contains sufficient iron and calcium to make it undesirable for the preparation of ultra high purity fluorides. The reaction product, NH_4F, can also create a problem. The NH_4F is given off as a gaseous product which condenses upon leaving the furnace. Care must be taken so that the outlet tube does not plug and that backstreaming of NH_4F can not occur. The most serious disadvantage occurs as a result of the water which is given off as a reaction product. The water from the reaction can collect in the salt bed giving rise to localized pockets of water vapor in contact with the fluoride. The hydrolysis reaction can then take place giving rise to the formation of the oxyfluoride. During the course of this investigation the oxygen content of materials produced by this technique was found to be higher than the oxygen content in corresponding fluorides produced by the anhydrous HF process.

Dehydration of the hydrated fluoride

This method utilizes the fact that the rare earth fluorides are insoluble in most aqueous media including those containing HF. The hydrated rare earth fluoride is usually precipitated from an aqueous solution of the oxide dissolved in either nitric or hydrochloric acid. The precipitate of the hydrated fluoride is filtered, dried and then thermally decomposed to yield and anhydrous fluoride.

Several difficulties have been found to be associated with this technique. The hydrated rare earth fluoride precipitates tend to be gelatinous and difficult to filter. However, with the proper techniques (8,17,20,29), easily filtered precipitates may be obtained. It is also possible to pick up impurities during the filtration and drying processes.

The most difficult problem associated with this technique is the removal of the one half mole of water of hydration (30) associated with the filtered precipitate. Smutz et al. (8) have shown that temperatures of 600°C. and above are needed to completely dehydrate the fluoride. Love (30) has shown that oxyfluoride formation becomes appreciable at temperatures of about 600°C. The hydrolysis reaction coupled with any unreacted oxide that may have been trapped in the precipitated, dried fluoride probably explains the slightly higher oxygen content (7) in fluorides prepared by wet versus dry methods.

Analyses of rare earth fluorides prepared by any of the above techniques have shown that the oxygen concentration was

in the range of 100-3000 ppm by weight. The maximum level of each metallic impurity was less than 20-30 ppm by weight with most impurities near or below their detection limit. However, the fluorides prepared by the ammonium bifluoride process sometimes contained iron and calcium impurities in excess of 50-100 ppm by weight.

All metallic impurities could be reduced to near their detection limites by using higher purity oxides and properly designed hydrofluorination equipment. However, it was necessary to remove the oxygen from the fluoride by some purification process.

The oxygen is probably present in the fluoride as either unreacted oxide and/or oxyfluoride formed during the conversion reaction. It should, therefore, be possible to lower the oxygen content by finding a set of reaction conditions such that all of the oxide will react and any oxyfluoride will be converted back to the fluoride.

In their attempts to prepare optical quality fluorides, others (26,27,28) have shown it was possible to reduce the oxygen content of LaF_3 by passing HF over the fluorides at high temperatures. A reduction in oxygen content was also achieved by passing HF over a molten mixture of the rare earth fluorides and LiF (24).

In view of the above considerations, the fluorides were prepared by a two-step process in this work. The reaction of anhydrous HF with the oxide was used to prepare the "raw"

fluoride. The "raw" fluoride was then topped in an atmosphere of HF and argon at temperatures above its melting point to reduce the oxygen content to less than 50 ppm. It was felt that this two-step process would introduce the least number of impurities and would produce the best quality fluorides.

EQUIPMENT

The following criteria were used in the design of the furnaces used to convert the rare earth oxides to their respective fluorides and to purify (top) the resulting fluorides:

(1) the maximum capacity of the furnace was to be on the order of 500 grams of material.

(2) there was to be minimal contamination of the fluorides by reaction of HF with the materials of construction.

(3) the furnaces were to be designed in such a way that possibilities of HF leakage were minimal.

(4) some provisions were to be made so that HF could be removed from the exit gas stream without backstreaming effects.

(5) provisions were to be provided so that the personnel and equipment would be protected in spite of a malfunction in some part of the furnace or supporting equipment.

To minimize danger to personnel, the furnaces were placed in large, walk-in hoods equipped with blowers of sufficient size to provide an air flow with a linear face velocity of 140 feet per minute. A safety interlock system was installed to automatically shut down all electrical power and the HF flow in the event of a change in any of the monitored parameters.

ıe air flow in the hoods was monitored by a vane switch. The cooling water and water to the scrubbing columns were monitored by a flow switch. In the event of a decrease in air flow (or water flow), the vane switch (or flow switch) activated the interlock system. Once activated, the system tripped magnetic circuit breakers to automatically turn off the electrical power to the furnaces and closed a Teflon solenoid valve attached to the regulator of the HF tank to stop the HF flow. The interlock system could also be activated manually with a mushroom switch located just inside the door to the room. After shut down, the furnaces could only be restarted manually.

In order to minimize the possibility of introducing impurities into the rare earth fluorides during the conversion or topping processes, materials of construction were selected which were nonreactive to HF. Copper was used to carry the HF at room temperature, and Monel, Inconel and nickel were used for all parts that were exposed to HF at temperatures above room temperature but less than 300^{o}C. Graphite, platinum or molybdenum were used in all areas in contact with the HF at temperatures over 300^{o}C.

The temperatures in both systems were measured by a series of platinum versus platinum-13% rhodium thermocouples. The emf outputs of the thermocouples were recorded with a 24 point, recording potentiometer made by Honeywell.

Conversion Furnace

A schematic diagram of the furnace used to convert the rare earth oxide to the fluoride is shown in Figure 1. The furnace consisted of a 4 inch I.D. platinum lined Inconel tube (E) heated by a Lindberg Hevi-Duty three zone electrical resistance furnace. The oxide charge was contained in a platinum boat which was then placed on the thermocouple well of the backplate (F). Both the thermocouple well and backplate were also covered with platinum. The backplate assembly was supported on a wheeled cart (C) which also held two argon tanks (K) and the HF tank which was enclosed in a steel box (J). The backplate and cart assembly were moved up to the furnace tube by a screw-type automotive jack (B) fastened to the cart. The screw was driven with a V-belt drive assembly (A) powered by an electric motor. The backplate was fastened to the furnace tube with eight bolts. A Teflon gasket (M) was used between the platinum liner of the furnace tube and the platinum jacket on the backplate assembly. The HF and argon flows were adjusted using Monel valves and the flows were measured with Kel-F rotameters. The HF-argon gas mixture was introduced at room temperature into the furnace tube through an Inconel fitting (L). The outlet gas from the furnace tube passed through a one half inch platinum tube (N) into a scrubbing column (G) where the HF was removed, then into a set of baffles (H) which removed entrapped water from the outlet gas stream. A slight negative pressure was maintained in the scrubbing

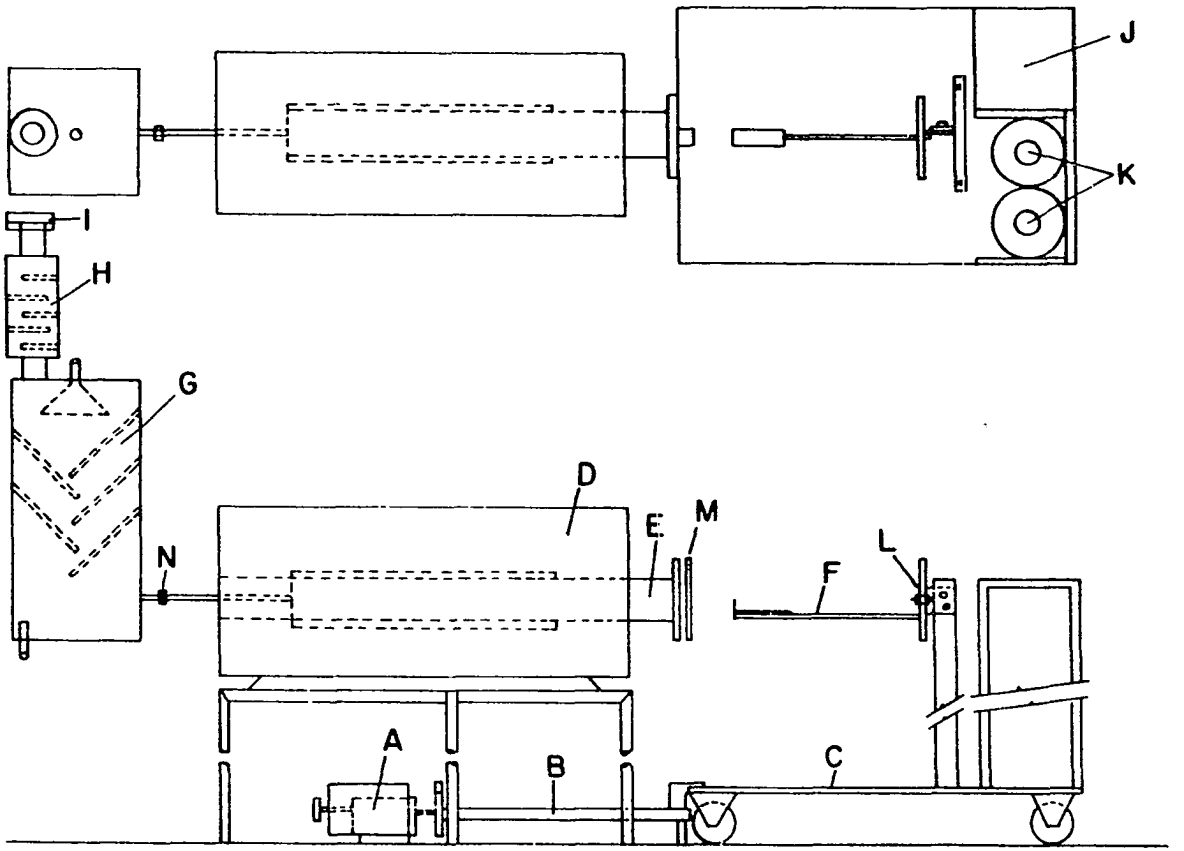

Figure 1. Schematic of the conversion furnace

column through the use of a small fan (I). The cleaned exhaust gas was then allowed to go up the hood vent while the very dilute aqueous HF was put down the drain.

The Topping Furnace

A schematic diagram of the topping furnace is shown in Figure 2. The furnace assembly consisted of a water cooled copper jacket (I) which was covered top and bottom with water cooled brass plates (J). The sample and HF atmosphere were contained in a graphite can (O). The graphite can was heated by means of a graphite heating element (L) powered by a step-down transformer with a rated maximum output of 10 volts at 2000 amperes. The heating element was supported by the electrical bus bars providing power to the heater. The bus bar assemblies were made up of a stack of 1½ by 2½ inch molybdenum strips approximately one half inch thick (K) fastened to the heater with molybdenum bolts and to a water cooled copper pipe (H). The copper pipe passed through an air tight, electrically insulated seal in the bottom plate of the furnace. Power was transferred from the transformer to the bus bar assembly by means of four strands of 4/0 welding cable. The lower third of the furnace was insulated with coarse Al_2O_3 (N) while the top of the furnace was insulated with graphite felt (M). The graphite can assembly (O) was supported by two graphite tubes (Q) which were sealed to the lid of the can, passed through the can support plate (P) and attached to the HF-argon inlet

and outlet fittings (R).

Outlet gas from the topping furnace was fed into a scrubbing column through an Inconel fitting (G). The scrubbing column consisted of a 5-inch Inconel outer tube (A) packed with pieces of 1-inch diameter by 2 inches long polyethylene tubing supported on a porous Inconel plate (C). Water was let into the column through an Inconel shower head (D) which was welded to the top plate of the column. A Teflon gasket (E) was used to seal the top plate. A small fan (E) attached to the exhaust has outlet provided a slight negative head in the scrubbing column.

Figure 3 shows a more detailed view of the graphite can used to contain the fluoride and the HF atmosphere. The can (A), the lid (C) and the tubes (D) were made from a high density, high purity graphite. The seal between the can and the lid was made by machining the bevel on the lid at a slightly steeper angle than the bevel on the can, thereby causing a line seal between the two beveled edges. The fluoride was contained in a deep-drawn, seamless platinum crucible (B).

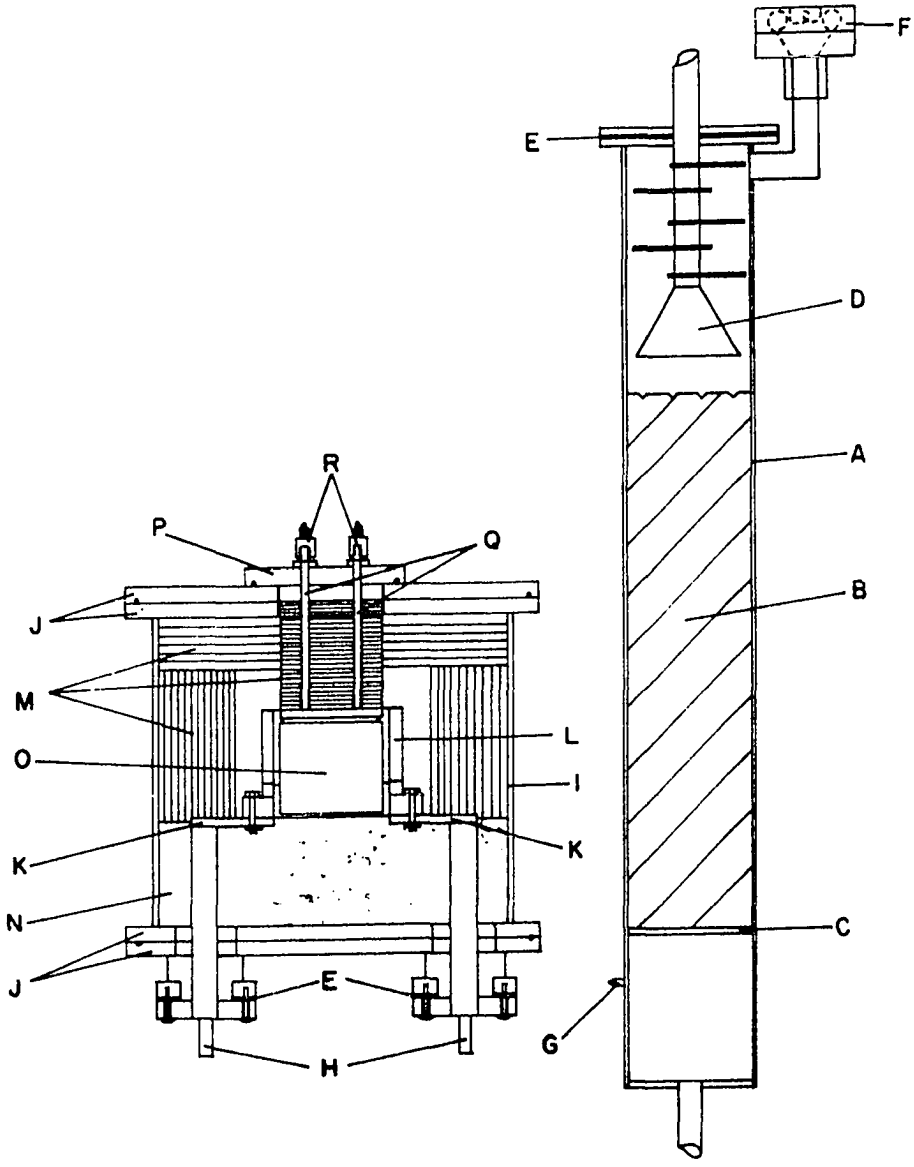

Figure 2. Schematic of the purification furnace

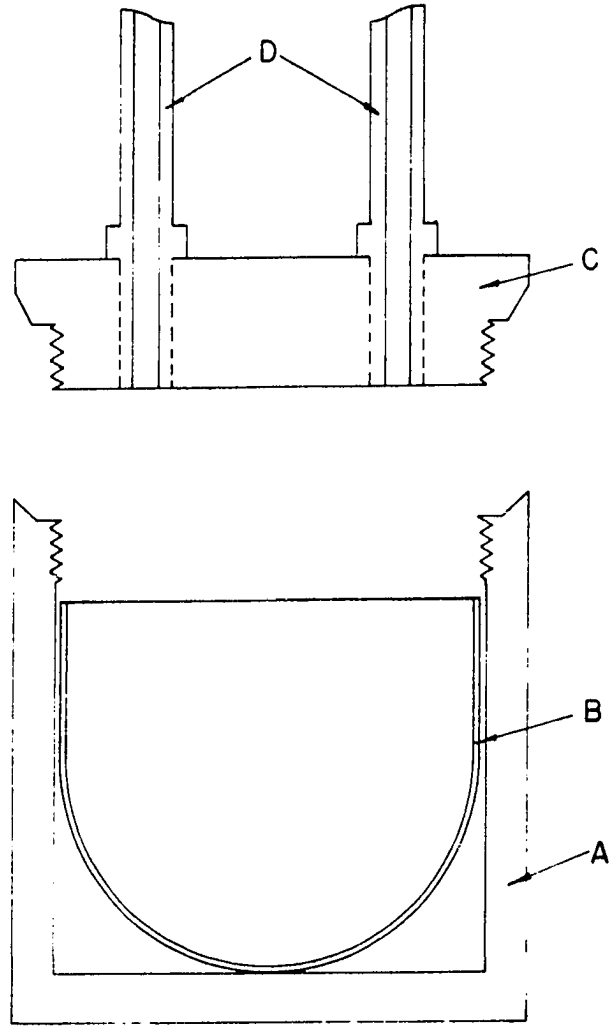

Figure 3. Schematic of the graphite can used with the purification furnace

MATERIALS

In order to minimize the number of variables which could affect the purity of the fluorides, a uniform supply of materials was used during this investigation. The source and purity of these materials are given below.

Platinum: The boats and crucibles used to contain the rare earth fluorides were fabricated from platinum reported by the manufacturer to be 99.999% pure. The conversion furnace liner was made from platinum that had been recovered from platinum scrap contaminated with thorium and graphite. Analysis of the recovered platinum showed the thorium and graphite content to be less than 2 ppm. Before use, the platinum parts were leached with hot sulfuric acid and heated to above their normal operating temperatures in the presence of a rare earth fluoride to remove any materials that might later be picked up by the fluorides.

Graphite: All graphite used in the construction of the topping furnace was grade AUC purchased from National Carbon Company. Volatile materials were removed from the finished graphite parts by heating the part to well over its normal operating temperature in the presence of a rare earth fluoride and a dynamic HF atmosphere.

HF: The anhydrous HF was purchased from the Matheson Company in twenty-five pound cylinders. Matheson reported the purity as 99.9%. No direct analytical check of the purity of the gas

could be made due to a lack of equipment and available techniques.

Argon: The argon was purchased from Air Products Company as a compressed gas of 99.995% purity. Analysis of the gas for oxygen and water showed it contained less than 3 ppm and 1 ppm by weight respectively. No further checks were made on the purity of the gas.

Rare earth oxides: The rare earth oxides were obtained from Dr. Powell's Physical and Inorganic Chemistry Group. These oxides were separated and purified by an ion exchange method described by Powell and Spedding (31). The oxides were taken from the middle two thirds of the band and were thoroughly homogenized before being analyzed. The typical concentration range of impurities in the rare earth oxides used in this work is given in Table 1. All analyses were done with the mass spectrograph except for N, C, Fe and Cu which were determined by wet chemical methods. All elements not listed were either undetected or present in concentration of less than 1 ppm by weight.

Table 1. The analysis of a typical rare earth oxide in ppm by weight

Impurity	Concentration Range[a]	Impurity	Concentration Range[a]
N	5 - 75	La	N.D. - 10
F	.03 - 2	Ce	N.D. - 10
Mg	N.D. - 10	Pr	N.D. - 10
Al	.2 - 5	Nd	N.D. - 10
Si	5 - 30	Sm	N.D. - 10
Cl	5 - 50	Eu	N.D. - 10
Ca	.5 - 20	Gd	N.D. - 10
Cr	.2 - 1	Tb	N.D. - 10
Mn	.1 - 1	Dy	N.D. - 10
Fe	3 - 10	Ho	N.D. - 10
Ni	.05 - 1	Er	N.D. - 10
Cu	.1 - 2	Tm	N.D. - 10
Pb	.5 - 10	Yb	N.D. - 10
Sc	N.D. - 2	Lu	N.D. - 10
Y	N.D. - 2		

[a]The larger number represents the maximum level found in any of the oxides used in this work. N.D. means not detected.

PROCEDURE

The procedures presented below are only the general manipulations required to operate the furnaces. The optimum conditions for preparing the fluorides will be given in the next section.

Preparation of the Anhydrous Fluorides

The rare earth oxides were contained in the platinum boat. The boat was positioned on the backplate assembly of the conversion furnace which was then bolted to the furnace tube. The water for cooling the furnace and for the scrubbing column was turned on. The furnace tube was purged with argon and then the argon flow through the tube was adjusted to the desired level. The furnace was brought to temperature by adjusting each of the three variacs which controlled the power input to the center and the two end heating zones. The heating zone nearest the gas inlet was operated about 50°C. hotter than the center zone and the heating zone nearest the gas outlet was adjusted to compensate for any end heat losses so that the temperature in the center zone was uniform. After the furnace reached the desired operating temperature, the HF flow was adjusted to the required level.

At the end of the run, the power to the furnace was turned off. When the temperature of the center zone dropped below 500°C., the HF flow was shut off but the argon flow was continued. After the furnace and its contents reached room temper-

ature, the fluoride was removed from the furnace and stored in plastic bags.

Purification of the Anhydrous Fluorides

The rare earth fluorides were purified (topped) by packing the fluoride from the conversion furnace into a seamless platinum crucible. The crucible was then sealed in the graphite can of the topping furnace and positioned in the furnace. The feed and exit lines for the HF-argon gas mixture were connected.

After the cooling water and the water to the scrubbing column had been turned on, the interior of the furnace was purged with nitrogen. The nitrogen flow was then adjusted to approximately 10 standard liters per hour (SLPH) to provide a protective atmosphere for the graphite parts. The argon flow to the inside of the graphite can was adjusted to the desired level. After about five minutes, the electrical power to the heater was slowly increased until the graphite can and its contents reached a temperature of 100 to 150 degrees above the melting point for the fluoride being run. The HF flow was then adjusted to the desired level.

After six to eight hours, the electrical power was slowly reduced. After the furnace had cooled to about 600^{o}C., the HF was shut off and the argon flow was increased. Once room temperature was achieved, the topped fluoride was removed

from the furnace and stored in plastic bags which were then sealed in jars filled with argon.

EXPERIMENTAL RESULTS

Preparation of the Anhydrous Fluorides

Since the conversion of the rare earth oxide to its fluoride depended on the reaction of a gas with a packed solid bed, conditions which would give the optimum yield might be expected to vary considerably. For instance, some of the conditions which could possibly affect the optimum yield were the depth of the oxide in the boat, the temperature of the reaction, the ratio of argon to HF, the flow rate of the HF-argon mixture and the length of the run. To optimize some of the parameters, experiments were conducted with 50 gram batches of oxide.

Since Carlson and Schmidt (7) had previously reported that good quality fluorides could be obtained by carrying out the reaction at temperatures of 700°C. during eight hour runs, the ratio of argon to HF and the total flow rates were determined under these conditions.

A total flow of 10 SLPH was selected to assure an adequate flow to carry off reaction products and to supply an excess of at least 200% of HF. The argon-HF ratio was varied from pure HF to a ratio of three parts argon to one part HF by volume. When pure HF was used, the resulting fluoride tended to compact together to form a solid mass. As the argon flow was increased, less compacting took place until at about a 1:1 ratio, the fluoride remained loose and granular in nature.

At higher argon to HF ratios, no improvement in either the appearance of the fluoride or the oxygen content was found.

Using a flow rate of 10 SLPH of a 1:1 ratio of HF to argon, and a eight hour run, the temperature of the center zone of the furnace was varied from 600 to 900°C. at fifty degree intervals. It was found that the oxygen content of the fluoride decreased slightly with temperature up to about 750°C. Beyond 750°C., the decrease in oxygen content was not sufficient to warrant the use of the higher temperature.

Using a flow rate of 10 SLPH, a HF-argon ratio of 1:1 and a furnace temperature of 750°C., the length of the run was varied from four to twelve hours in one hour increments. It was found that the oxygen level in the fluoride decreased with respect to the length of the run until seven to eight hours had elapsed. Beyond seven to eight hours, no significant decrease in oxygen content was found.

As a result of the above experiments the best conditions for converting 50 gram batches of rare earth oxide to the fluoride appeared to be an eight hour run at 750°C. with a 1:1 ratio of HF to argon at a total flow at 10 SLPH.

Since the ultimate goal was to be able to convert batches of 500 grams of oxide to the fluoride, the process was scaled up to permit this. The total HF-argon gas flow was increased to 100 SLPH and the depth of the oxide bed was changed from ¼ inch to 1 inch to accommodate the increase in capacity. Using the above conditions, a good quality fluoride could be

made from all of the rare earth oxides. The oxygen content as determined by a helium fusion technique (32) was between 100 and 300 ppm by weight. No other chemical analyses were made of these materials at this point.

Purification of the Fluorides

The fluoride contained some unreacted oxide and oxyfluoride formed by hydrolysis during the conversion step. To reduce the oxygen level, the fluorides were reacted with anhydrous HF at temperatures above their melting points. Under these conditions any oxide present reacted completely and the equilibrium of the hydrolysis reaction (equation 10) was shifted to the right giving the pure trifluoride. However, it was necessary to determine the optimum conditions to obtain the highest purity fluorides.

A flow rate of 100 SLPH of a 1:1 ratio of HF and argon was used. The temperature and length of time of the run were varied to determine their effect on the oxygen content. It was found that a temperature of approximately 100°C. over the melting point of the fluoride and a run of six to eight hours produced the best fluoride. Higher temperatures and longer runs did not make any noticeable difference in the purity of the fluorides.

The above conditions were found to be suitable for the purification of YF_3 and lanthanum through lutetium fluorides inclusive with the exception of EuF_3. For some reason which

was not apparent, this process produced europium fluoride which was a mixture of the divalent and trivalent states.

The purified fluorides were analyzed for oxygen content by the helium fusion method. The other impurities were determined by a mass spectrographic technique with the exception of carbon and the total rare earth and fluoride contents, which were determined by wet methods. The oxygen content was found to be less than 50 ppm by weight for all purified fluorides and less than the detection limit (20 ppm) for most of the batches. No apparent impurities were added during either the conversion or purification step. A complete analysis of YF_3, LaF_3, PrF_3, NdF_3, GdF_3 HoF_3 and LuF_3 is given in Appendix A. The analyses of the other fluorides are similar.

SUMMARY

A technique to prepare high purity rare earth fluorides has been devised. The rare earth oxide was converted to the trifluoride by passing a mixture of anhydrous HF and argon over a bed of the oxide at 750°C. The converted fluoride contained some unreacted oxide and some oxyfluoride formed by the reaction of the fluoride with water given up as a reaction product during the conversion process. By use of the proper techniques, the oxygen content could be limited to 100 to 300 ppm.

To further reduce the oxygen content, it was necessary to react the molten fluorides with HF. In the presence of HF and at the high temperatures necessary for the fluorides to be in their molten state, any unreacted oxide was completely converted to the fluoride. At the same time, the oxyfluoride hydrolysis reaction was reversed, thereby converting the oxyfluoride back to the pure fluoride. This purification process (topping process) lowered the oxygen content to less than 50 ppm for all batches of fluorides and to less than the detection limit for most batches. Further analyses showed that no significant amounts of other impurities were added during either the conversion or topping processes.

The fluorides prepared by this two-step process were completely transparent, qualitatively indicating that no unreacted oxide or oxyfluoride was present. After reacting

with HF in the molten state, the fluorides were quite stable with respect to contact with air. No increase in the oxygen content was detected in topped fluorides exposed to air for periods of up to six months.

PART II. SOME HIGH TEMPERATURE PROPERTIES OF THE RARE EARTH TRIFLUORIDES

REVIEW OF THE LITERATURE

Although the rare earth trifluorides have been prepared by many people, few of their properties have been determined. This review will be limited to only the measurement of the high temperature properties of the rare earth trifluorides; that is, those properties which were determined above room temperature.

The melting points of the rare earth trifluorides have been reported in handbooks for many years with differences in listed melting points sometimes varying by as much as 200°C. Dennison of the Ames Laboraotry determined the melting points of the trifluorides by differential thermal analysis (DTA) in the early 1960's. His values were regarded as some of the best available and were cited in the literature by Carlson and Schmidt (7).

Dennison also found a second thermal arrest for some of the fluorides while making the DTA runs. This second thermal arrest, which occurred at temperatures below the melting point, was attributed to the crystalline transformation from the low temperature orthorhombic form to the high temperature hexagonal form. Dennison did not observe a crystalline transformation for LaF_3, CeF_3, PrF_3, NdF_3, TbF_3, DyF_3 and HoF_3.

Thoma and Brunton (33) studied the orthorhombic to hexagonal crystalline transformation with the aid of a high temper-

ature x-ray diffractometer. Their results were in good agreement with those of Dennison with the exception of TbF_3, DyF_3 and HoF_3. They found that TbF_3, DyF_3 and HoF_3 also underwent a orthorhombic to hexagonal transformation upon heating. They further speculated that LaF_3 through NdF_3 might also undergo the transformation at low temperatures although they were not successful in finding such a transformation even at liquid nitrogen temperatures.

The crystal structure of the light rare earth fluorides was first reported in 1931 by Oftedal (34,35) who proposed a structure based on single crystal x-ray studies of the mineral tysonite. The presence of weak reflections led Oftedal to believe the crystal structure belonged to the hexagonal space group $P6_3/mcm$. In 1953 Schlyter (36) failed to see these faint reflections in tysonite crystals and proposed a smaller unit cell belonging to the space group $P6_3/mmc$, but Templeton and Dauben (37) found the weak reflections in CeF_3. Recent single crystal x-ray studies of high purity LaF_3 by Zalkin and Templeton (38) and Mansmann (39,40) have shown that, although the larger cell of Oftedal was correct and that his coordinates for La were accurate, the crystals were of a trigonal symmetry rather than hexagonal. They proposed a trigonal cell belonging to the space group $P\bar{3}c1$. Lattice parameters, determined by powder techniques, of the room temperature hexagonal (or trigonal) form of the rare earth fluorides have also been reported by Zalkin and Templeton (41) and Staritzky and Asprey (42).

Zalkin and Templeton (41) determined the crystal structure of YF_3 from single crystal x-ray data. They found it to be orthorhombic belonging to space group Pnma. In addition, Zalkin and Templeton found the room temperature modification of the trifluorides of samarium through lutetium to be orthorhombic. However, they were also able to quench in a high temperature modification in SmF_3, EuF_3, HoF_3 and TmF_3 which they reported to be hexagonal. Staritzky and Asprey (43) have determined the lattice parameters of the orthorhombic form of YF_3, SmF_3 and YbF_3 by powder techniques and their results are in good agreement with those of Zalkin and Templeton.

Prior to 1965, no reliable experimental thermodynamic data was available for the rare earth fluorides with the exception of cerium fluoride. Since 1965, there have been only a limited number of thermodynamic studies. These have consisted mainly of vapor pressure work.

Margrave and co-workers (44-49) have measured the vapor pressure of ScF_3, YF_3, LaF_3, CeF_3, NdF_3, DyF_3, HoF_3, ErF_3, TmF_3, YbF_3 and LuF_3 over a temperature range of approximately 1100 to 1500^{o}K. by both microbalance studies and mass spectrometric techniques. From this data they have calculated the enthalpy and entropy of sublimation. Mar and Searcy (50) and Lim and Searcy (51) have also measured the vapor pressure of LaF_3 and CeF_3, respectively. Their results are in good agreement with those of Margrave and co-workers. Suvorov et al.

(52) have measured the vapor pressure of LaF_3, CeF_3, PrF_3 and NdF_3 and their values are in reasonable agreement with the above data. Skinner (53) has also measured the vapor pressure of PrF_3.

The heats of formation of ScF_3, YF_3, LaF_3, NdF_3, GdF_3, HoF_3 and ErF_3 have been calculated from combustion data obtained from fluorine bomb calorimetry (54). Chaudhuri (55) has measured the heat content of CeF_3, PrF_3, NdF_3, GdF_3, DyF_3 and YbF_3 over a temperature range of 500 to 1400°K. The heat capacity, entropy and free energy functions as a function of temperature were calculated.

The thermodynamic properties of CeF_3 have been measured by King and Christensen (56) and Westrum and Beale (57). Low temperature thermodynamic data are available only for CeF_3.

METHOD AND THEORY

Method

The study of high temperature thermodynamic properties by calorimetric techniques demanded that certain requirements and restrictions be considered. Among these were the length of time required to obtain the data, the limits imposed on the equipment and sample by temperature, and the nature of the sample itself. A thermodynamic study of the rare earth fluorides at elevated temperatures placed primary emphasis on the latter two considerations. The reactivity of the fluorides with moisture in the atmosphere at elevated temperatures and the possibility of contamination from the sample containers required that the samples be protected by either an inert atmosphere or a vacuum or else be sealed in an inert metal such as platinum or tantalum.

Four general calorimetric methods currently used to determine the thermodynamic properties of pure materials are

(1) thermal analysis studies

(2) adiabatic methods which measure heat capacity directly

(3) transient or pulse techniques

(4) the drop method (method of mixtures).

Certain of the adaptations made of these methods will be briefly described and compared to one another.

Thermal analysis studies

The thermal analysis method consists of heating and cooling a massive sample at a known rate and measuring the change in temperature versus time. The rates are then either compared with those run under similar conditions on a known material, or compared directly with a known material by a differential technique. Although the method is rapid, unless elaborate precautions are taken its accuracy and reproducibility are limited and the results are usually semi-quantitative at best.

In spite of these drawbacks, Cavallaro (58) used this method to measure the heat of fusion of praseodymium metal in 1943. A modification of this method was described by Butler and Inn (59) in 1958. They determined the heat capacity of gold, silver, nickel, molybdenum, copper and platinum by heating the sample to 1000°C. in an evacuated chamber, and then allowing the sample to cool by radiation. The rate of cooling was followed by means of a thermocouple attached to the sample. They reported an accuracy of ± 5%.

A commercial instrument, the differential scanning calorimeter, which is another modification of this method, has recently become available. The instrument will operate over a range of -100 to 500°C. with a reported accuracy on the order of ± 1%.

Adiabatic methods

The adiabatic method is used to directly measure the heat capacity of a sample by adding a known amount of heat and observing the temperature rise. In order for this method to be reproducible and reliable, the sample must be maintained in adiabatic surroundings; that is, no heat can be gained or lost by the sample. This method has the advantages of giving accuate, reproducible results and having the capability of running continuously from lowest to highest temperature.

Since the problem of providing adequate shielding becomes extremely difficult at high temperatures, the adiabatic method is generally used only at low temperatures. However, in 1958 West and Ginnings (60) described an adiabatic calorimeter which could be used up to 600°C. In 1959, Stansbury et al. (61) measured the thermodynamic properties of nickel from 0° to 1000°C. using an adiabatic calorimeter with a reported accuracy of ± 0.5%. Although few adiabatic calorimeters have been operated at temperatures above 1000°K., Backhurst (62) described an adiabatic calorimeter that could be operated to temperatures of 1600°K. and Braun et al. (63) described an adiabatic calorimeter that could be operated to temperatures of 1800°K.

Transient techniques

The transient or pulse technique has been used when limitations due to container materials, temperature measurement,

and environment have eliminated other techniques. The transient technique utilizes a sudden pulse of energy to raise the sample to a very high temperature. The temperature is measured as a function of time and energy input. Several sources have been used to provide the energy pulse. Examples of some of these sources are the electrical pulse provided by the discharge of a capacitor, the use of an arc image furnace, a bright light flash and the laser beam. The temperature is determined by a resistance-temperature relationship as a function of time or by a photoelectric pyrometer.

Worthing (64) was the first to use the pulse technique for specific heats of metals, and later Avramescu (65) and others (66) also used this technique.

The drop method

The drop method, or the method of mixtures, as it is commonly called, consists of dropping the sample from a furnace into a calorimeter operating at or near room temperature. In this manner the heat content (enthalpy) of the sample between the temperature of the sample in the furnace and the final equilibrium temperature of the sample in the calorimeter is measured.

Several types of calorimeters have been used. These may be of the ice type used by Spedding et al. (67), the water type used by White (68), or the metal block type used by Jaeger and Rosenbohm (69), Southard (70), and Kelley, Naylor

and Shomate (71).

There are two main disadvantages of the drop method. First, the method is not always adequate for obtaining heat effects at transition points, especially if the heat of transition is small. The reason is that two large quantities of heat must be subtracted from one another to obtain the heat of transition. The total error in the large heat values also appears as the error in the sometimes relatively small difference. Second, it is necessary for the sample under investigation to revert to its original state upon cooling if it undergoes any changes upon heating. If it does not, equilibrium is not obtained and such data are not reliable.

Among the advantages of this method are that it is direct and reasonably rapid. The results are accurate within the limits of reproducibility in the behavior of the substance, and it depends on no extraneous assumptions.

The high temperature thermodynamic measurements of this work were done using an adiabatic copper block drop calorimeter and an induction furnace to heat the samples. The adiabatic copper block calorimeter has several advantages over isothermal calorimeters.

(1) It is relatively rapid as compared to isothermal methods.

(2) It is not necessary to obtain high purity ice or diphenyl ether and maintain a constant volume as would be necessary in isothermal calorimeters not

using a copper block.

(3) The calculation of the heat content of the sample is simplified.

(4) The heat content is measured relative to the copper block which is held in the vicinity of 298°K. which is the usual reference temperature for high temperature thermodynamic work.

Some disadvantages of the adiabatic copper block calorimeter are

(1) Adiabatic conditions must be maintained to obtain accurate data. This requires a relatively complex set of control circuits.

(2) To determine the heat content of the sample, it is necessary to measure small temperature differences in the massive copper block very accurately.

(3) The precision of the calorimeter decreases with an increase in heat liberated by the sample in the copper block due to increased difficulty in maintaining adiabatic conditions.

(4) An accurate calibration technique is required to determine the heat equivalent of the calorimeter.

This method was selected because of its advantages coupled with its successful operation in this laboratory. Most of the disadvantages were overcome by the proper selection of electronic circuitry and temperature measuring equipment.

Theory

As noted previously, the drop method is used to measure the enthalpy change of a sample at a known temperature relative to the block temperature. If the enthalpy change is then expressed as a function of temperature, other thermodynamic functions such as the heat capacity, the entropy and the free energy function can be calculated.

The measured heat content represents the change in enthalpy between the initial temperature of a sample in a furnace and the final temperature of the sample in the calorimeter. This enthalpy change can be represented by

$$\Delta H = H_T - H_{block} \tag{12}$$

where H_T is the enthalpy of the sample in the furnace and H_{block} is the enthalpy of the sample in the calorimeter block at the equilibrium temperature. However, the enthalpy and other thermodynamic functions are usually expressed relative to a standard temperature. In the case of high temperature work this standard temperature is usually 298.16°K. Therefore, the enthalpy values obtained with the drop calorimeter must be corrected to the standard thermodynamic reference temperature. If the room temperature heat capacity of the sample is known or can be estimated, the correction to the enthalpy can be found as follows:

$$\Delta H_{corr} = \int_{T_{block}}^{298} C_p \, dt \tag{13}$$

where ΔH_{corr} is the enthalpy correction, C_p is the heat capacity at constant pressure, T_{block} is the equilibrium temperature of the sample in the calorimeter and T is the temperature in degrees Kelvin. This correction is quite small in the case of adiabatic copper block calorimetry since the block temperature is maintained very near 25°C. at all times.

Although the enthalpy change is said to be measured at constant pressure, the pressure is not actually constant. The samples are sealed in crucibles under argon. Upon heating, the pressure in these crucibles can increase by five to ten atmospheres. The variation in enthalpy with pressure at constant temperature can be found from the relationship

$$\left(\frac{\partial H}{\partial P}\right)_T = -T\left(\frac{\partial V}{\partial T}\right)_P + V \qquad (14)$$

The coefficient of thermal expansion, α, is given by

$$\alpha = \frac{1}{V}\left(\frac{\partial V}{\partial T}\right)_P \qquad (15)$$

Substituting equation 15 into equation 14 and rearranging, we have

$$\left(\frac{\partial H}{\partial P}\right)_T = V\ (1 - \alpha T) \qquad (16)$$

In general this correction is quite small for most solids at the pressures encountered in drop calorimetry and may be neglected. The correction is on the order of ten to twenty calories per mole for the rare earth fluorides. This is well within the experimental error and will be neglected.

The standard enthalpy change can now be calculated by combining equations 12 and 13.

$$\Delta H^{o} = \Delta H + \Delta H_{corr} = H_{T}^{o} - H_{298}^{o} \qquad (17)$$

Various empirical equations may be used to express the standard enthalpy data as a function of temperature. The equation recommended by Maier and Kelley (72)

$$\Delta H^{o} = A + BT + CT^{2} + DT^{-1} \qquad (18)$$

will be used here for algebraically representing the heat contents above the reference temperature of 298.16°K.

The heat capacity of a material at constant pressure, C_p, is defined by

$$C_p = \left(\frac{\partial H}{\partial T}\right)_p \qquad (19)$$

Therefore, the heat capacity of the sample as a function of temperature calculated by differentiating equation 18 is

$$C_p = B + 2CT - DT^{-2} \qquad (20)$$

The expression for the heat capacity may then be used to calculate the change in entropy, ΔS, by using the relationship

$$\Delta S^{o} = \int_{298}^{T_{Tr}} \frac{C_p}{T}\,dT + \frac{\Delta H_{Tr}}{T_{Tr}} + \int_{T_{Tr}}^{T_{Mp}} \frac{C'_p}{T}\,dT + \ldots \qquad (21)$$

Combining equations 20 and 21, the entropy change can be calculated from the experimental data. For example, for $T < T_{Tr}$, equation 21 becomes

$$\Delta S^{o} = S_{T}^{o} - S_{298}^{o} = B\ln\left(\frac{T}{298}\right) + 2C(T - 298) + \tfrac{1}{2}D\left(\frac{1}{T^{2}} - \frac{1}{298^{2}}\right) \qquad (22)$$

The free energy function, $-(F_T^o - H_{298}^o)/T$, is defined as

$$-\left(\frac{F_T^o - H_{298}^o}{T}\right) = S_T^o - S_o^o - \left(\frac{H_T^o - H_{298}^o}{T}\right) \qquad (23)$$

where S_T^o is the entropy at temperature T, S_o^o is the entropy at 0^oK. and $(H_T^o - H_{298}^o)$ is the enthalpy calculated from equation 6. In order to calculate the free energy function, the quantity $S_T^o - S_o^o$ must be evaluated. Since data obtained from the drop method gives only $S_T^o - S_{298}^o$, $S_{298}^o - S_o^o$ must be estimated or obtained from low temperature calorimetry data.

The above formulas are the basis for expressing the thermodynamic data as determined by the drop method. It is sometimes possible to express the thermodynamic functions in more complex mathematical form by using rigorous derivations based on models of the solid state. However, at this time calculated or estimated thermodynamic data at high temperatures based on the solid state model are generally not reliable for most solid materials.

MATERIALS

The rare earth fluorides were prepared in the manner described in Part I. A complete analysis of the fluorides is given in Appendix A.

Due to its ease of fabrication and nonreactivity towards the rare earth fluorides, tantalum was used as the crucible material. The tantalum was purchased from Fansteel Incorporated in the form of sheet and tubing. Crucibles of the appropriate sizes were fabricated by inert gas welding and then outgassed to approximately 2000°C. under a vacuum of 10^{-6} torr before use.

The α-Al_2O_3 (corundum) was purchased from Linde Air Products as a fused cylindrical rod approximately ½-inch in diameter. Pieces broken from this rod were used in the calibration of the calorimeter.

The reference grade platinum and platinum versus 13% rhodium thermocouple wire were purchased from J. Bishop and Company. A representative thermocouple from each spool of wire was checked against a thermocouple calibrated by the National Bureau of Standards. This calibration was assumed to be good for the entire spool. High purity alumina insulators for use with the thermocouples were purchased from the Refractory Division of the Norton Company.

EQUIPMENT AND PROCEDURES

Equipment

Two adiabatic copper block drop calorimeters were used to measure the heat contents of the rare earth fluorides. The first was originally built by D. H. Dennison of this laboratory. Part way through the experimental measurements, several components of Dennison's calorimeter deteriorated to the point that the calorimeter no longer functioned properly. Rather than simply repair the calorimeter, numerous modifications were made in an attempt to improve its reliability and accuracy. Since many components of the two calorimeters were similar, the new calorimeter will be described in detail and then the differences between the two calorimeters will be pointed out.

A schematic diagram of the new calorimeter is shown in Figure 4. The drop calorimeter can be divided into two basic sections, the calorimeter itself and the external area where the sample is heated.

The gold plated copper block (F) of the calorimeter was a solid cylinder of copper weighing about 7½ pounds. A tapered well approximately 2½ inches deep was cut into the center of the block for the sample chamber. A copper disc, supported by a trip mechanism, formed a false bottom to the sample well. As the sample dropped into the well, it pushed the copper disc down to the true bottom, thereby activating

the trip mechanism and closing a massive copper lid to cover the opening of the well. The block was supported on two probes (A) which were the sensors for a model 2801A Hewlett Packard quartz thermometer.

The temperature of the copper block was measured with the quartz thermometer. The operation of the quartz thermometer was based on the sensitivity of the resonant frequency of a specially cut quartz crystal to temperature change. The temperature range of the quartz thermometer was -80 to 250°C. with the linearity being ± 0.05%. However, for use with the calorimeter, only temperatures between 20 and 30°C. were measured. The digital readout of this instrument gave direct temperature readings in degrees C. with a resolution of 0.01, 0.001, or 0.0001°C. The instrument was calibrated by Hewlett Packard and no further calibrations were carried out with the exception of a periodic check of the ice point. All temperature differences of the calorimeter block were measured to 0.0001°C.

A thin, gold plated copper shield (D) completely surrounded the copper block. The shield was supported and positioned by six Plexiglass spacers (E) on the bottom and five spacers on the top. A 2000 ohm manganin heater was attached to the shield and a ½-inch diameter hole was cut in the center of the top of the shield for the sample to pass through.

The block and shield were enclosed in a double wall stainless steel vacuum jacket (B). The flange (C) of the vacuum system was connected to a 4-inch oil diffusion pump

vacuum system capable of producing a vacuum of 10^{-6} torr. A copper optical baffle (H) was positioned in the vacuum port. To isolate the calorimeter from the heating zone of the furnace, a movable water cooled gate (G) was installed in the top of the vacuum jacket.

A block diagram of the control circuits for the adiabatic shields is given in Figure 5. Two noninteracting circuits were used for control of the inner, thin copper shield and the vacuum jacket which served as the outer shield.

The reference signal for the inner shield control circuit was provided by a 8-junction thermopile made of copper and constantan thermocouple wires. Each junction was electrically insulated with a varnish, wrapped in copper foil and securely attached to the copper block (or the inner shield) with small screws. One set of thermocouple junctions was spaced at regular intervals around the copper block. Of the remaining set, four junctions were attached to the side wall and two junctions were attached to both the top and bottom surfaces of the inner shield. The signal from the thermopile was bucked against the output from a set point station to give a difference signal which was fed into a 3-action controller. The set point station, the deviation amplifier and the 3-action controller were series-M units purchased from Leeds and Northrup Company. The signal from the controller determined the power output of a 20 watt Kepco solid state power supply to the heater wound on the inner shield.

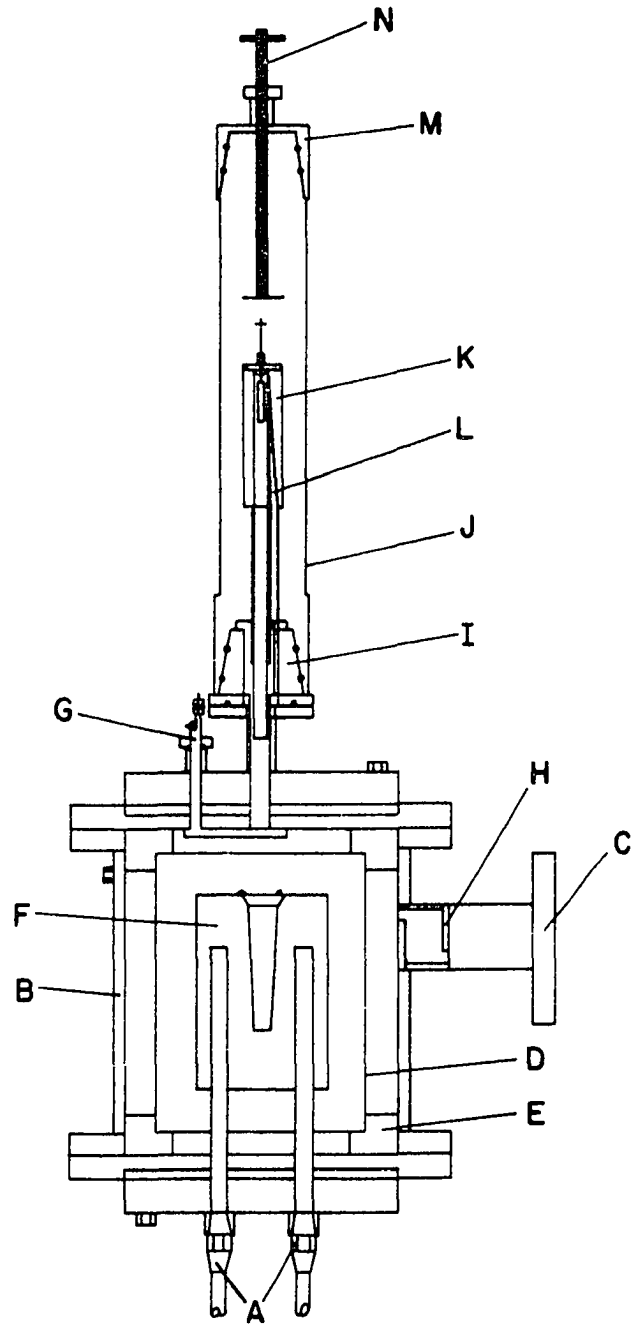

Figure 4. Schematic diagram of the adiabatic copper block drop calorimeter

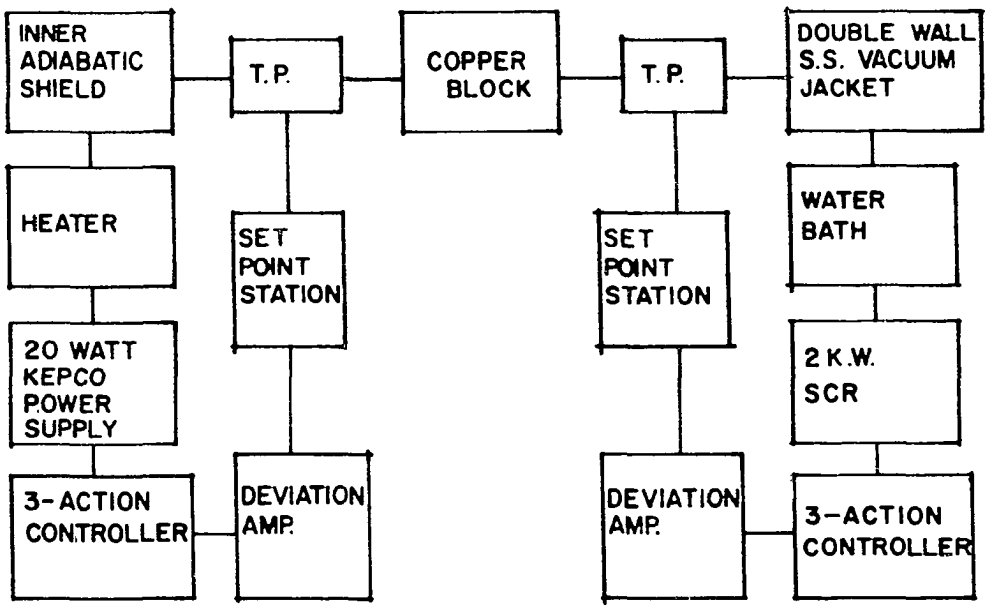

Figure 5. Block diagram of the calorimeter control circuits

The reference signal for the outer adiabatic shield control circuit was provided by a 6-junction thermopile made of copper and constantan thermocouple wire. Each junction was electrically insulated with a varnish, wrapped in copper foil, and securely attached to either the block or the vacuum jacket. The signal from the thermopile was bucked against the output from a set point station to give a difference signal which was amplified with a deviation amplifier and then fed into a 3-action controller. The set point station and the deviation amplifier were series-M units while the controller was a series 80 unit. All were purchased from Leeds and Northrup. The signal from the controller determined the power output of a 2 K.W. silicon controlled rectifier (SCR) which provided power to two 1000 watt heaters. The heaters were installed in an insulated, stirred water bath with a capacity of about 7.5 gallons. The SCR also controlled a solenoid switch in the cooling water line to the water bath in such a manner that when the heaters were on, the cooling water was off and when the heaters were off, the cooling water was on. The water from the bath was pumped between the walls of the calorimeter vacuum jacket with a centrifugal pump which had a pumping capacity of about five gallons per minute.

The external parts of the calorimeter are described below. The identifying letters associated with the components refer to Figure 4.

The sample and crucible, which together weighed about

ten grams, were suspended from a pair of tantalum fingers attached to a molybdenum lid. The lid was secured by four molybdenum screws to the top of a molybdenum cylinder (K) 3/4-inch O.D by 7/16-inch I.D. by 3 inches long which acted as the susceptor for the RF field of the induction heater and as a heat sink for the sample. A thermocouple well (L) was bored through the molybdenum block at an angle so that the thermocouple junction was forced against the side of the sample crucible.

The molybdenum block was supported by a tantalum pedestal which was fastened into a brass block. The brass block holding the pedestal was supported by a water cooled brass taper (I). A Vycor tube (J) was mated at each end with the water cooled brass tapers (I,M) to form a vacuum seal. The top brass taper (M) was equipped with a movable plunger (N). The plunger was used to push a tungsten rod in the lid of the molybdenum block which in turn spread the tantalum fingers and allowed the sample to drop.

The molybdenum block containing the sample was heated using induction heating. The induction unit was a 20 K.W. RF converter manufactured by the Ecco Corporation. The operating frequency was 450-500 kilohertz. A constant temperature of $\pm$ 3^{o}C. could be maintained along the full length of the molybdenum block. Blowers were provided to cool the Vycor tube.

The temperature of the sample was measured with a platinum versus platinum-13% rhodium thermocouple which was

inserted into the well in the molybdenum block. The thermocouple was shielded with tantalum to prevent the pick-up of stray signals from the RF field. The output of the thermocouple was continuously monitored by a recording potentiometer while the actual emf was measured periodically using a Leeds and Northrup K-4 potentiometer. With this set-up, the temperature could be accurately read to within ± 1°C.

Dennison's calorimeter was similar to the one described above. The major differences were in the control systems and the method used to measure the block temperature. Matched copper resistance thermometers wound on the block and the shields were used as the sensing elements for a light beam galvanometer controlling device. High wattage photoconductors activated by the light beams supplied a variable amount of power to the heater on the inner shield and regulated an on-off hot water valve on the circulating water system attached to the vacuum jacket. A modified Kelvin bridge circuit was wound on the copper block to measure the temperature.

Procedure

Operation of the calorimeter

The control circuitry and quartz thermometer were turned on and allowed to warm up. During the warm up period, the trap door of the copper block was set in the open position and the sample to be run was positioned in the molybdenum block. The thermocouple was placed in its well as the molybdenum

block assembly was positioned in the vacuum jacket of the calorimeter and then the thermocouple shield was put in place. The replacement of the Vycor tube and top cap completed the calorimeter assembly.

The calorimeter was evacuated to a pressure of approximately 10^{-6} torr. The converter was turned on and the sample was heated to slightly above the desired temperature. After the sample reached temperature, the calorimeter was backfilled with argon to a gauge pressure of approximately -25 inches of water and the sample was allowed to reach an equilibrium temperature.

After the sample had been at the equilibrium temperature for at least thirty minutes, the temperature of the block was monitored for a period of ten minutes to determine the initial drift rate. At the end of the ten minute period the sample temperature was measured and the sample was dropped into the calorimeter. The water cooled gate on the vacuum shell was opened just long enough for the sample to pass by it into the copper block.

The sample was allowed to come to equilibrium with the block, which usually took about ten minutes. The final block temperature was noted and the drift was again measured for a ten minute period. After each run, the sample was removed from the copper block and the above procedure was repeated.

At the end of the day, or whenever the block temperature

exceeded 28°C., the shield controllers were turned off and the copper block was allowed to cool. For all runs, the temperature of the copper block was kept between 22 and 28°C.

Calculation of the heat content

In a true adiabatic system, no heat is lost or gained by the system. However, in real systems it is impossible to obtain truly adiabatic conditions. Therefore, to compensate for any heat losses in the calorimeter, the shield controls of the calorimeter were adjusted so that the temperature of the block increased slowly (about 0.0001°C. per minute) at all times.

The calculation of the heat content of the sample depended on knowing the temperature rise of the copper block after the sample was dropped into the block. Since the temperature rise would include the effect of the sample plus any heat leaks in the calorimeter, it was necessary to compensate for the heat leaks in order to determine the true temperature rise of the copper block. This was done by measuring the drift rate of the copper block, i.e. the change in temperature of the block with respect to time, before the sample was dropped into the block (initial drift rate) and after the sample came to thermal equilibrium with the block (final drift rate). The initial drift curve and final drift curve were extrapolated to the middle of the nonequilibrium period and the difference between the two drift curves was taken at that point. This difference

represented the temperature rise of the block corrected for the drift rate. The correction due to the drift rates was usually on the order of about 1% or less.

Calibration of the calorimeter

In 1949, the U.S. Calorimetry Conference recommended the use of α-Al_2O_3 as the high temperature standard for the comparison of calorimeters. The heat content of α-Al_2O_3 as determined by Furukawa et al. (73) of the National Bureau of Standards is usually used as the basis for comparison of data.

The drop calorimeter was calibrated using α-Al_2O_3. Using a sample of α-Al_2O_3, a series of drops was made from the same temperature. From these drops, the heat equivalent of the calorimeter was calculated. The heat contents of two additional α-Al_2O_3 samples of different weights were then measured over the temperature range of 100 to 1000°C. and the results were compared with the National Bureau of Standards data as a check of the calibration.

Two other considerations were taken into account in the calibration of the drop calorimeter. Since the sample was contained in a crucible, the sum of the heat contents of the sample and the crucible was measured. Therefore, the heat content of the crucible had to be known as a function of temperature in order to calculate the heat content of the sample. Also, some heat was lost by the sample and crucible between the time they left the hot zone of the furnace and the time

they entered the adiabatic conditions of the calorimeter. Both factors were accounted for by making a series of drops to determine the heat content of the empty crucibles as a function of temperature. In this manner, the measured heat content of the empty crucibles included any heat losses which occurred during the drop. It was then assumed that the heat losses for a crucible containing a sample were the same as for the empty crucible.

RESULTS

Physical Properties

In the characterization of a material, the physical properties such as the melting point, the transition temperature, and the lattice parameters are usually among the first properties to be determined. Although these properties have previously been measured (7,38,39,41) for the rare earth trifluorides, the transition temperatures, the melting points, and the room temperature lattice parameters were determined again using the higher purity materials described in Part I.

The transition temperatures for the orthorhombic to hexagonal transition and the melting points of the rare earth trifluorides were determined by differential thermal analysis. The thermal analysis determinations were carried out by sealing the fluoride sample under 2/3 atmosphere of helium in a tantalum crucible ½ inch in diameter by 1¼ inches long. The crucibles were fabricated with a thermocouple well into which a platinum versus platinum-13% rhodium thermocouple was inserted to measure the temperature. The reference was a tantalum crucible containing lutetium metal. Thermal gradients were minimized by supporting the crucible on the thermocouple inside a molybdenum block which was positioned in the central zone of a tantalum resistance furnace. The heating and cooling rates were 5°C. per minute.

The emf of the thermocouples was measured with a Leeds

and Northrup K-3 potentiometer. The thermocouples were originally calibrated against a National Bureau of Standards calibrated thermocouple and the melting point of a copper standard was determined before and after each run as an additional check.

On heating, the thermal arrests were isothermal within the experimental error of ± 3°C. for both the transition temperatures and the melting points. The thermal arrests on cooling were not used because of observed supercooling of the samples. The amount of supercooling was sometimes as much as 60 to 70°C.

The transition temperatures and the melting points of the rare earth trifluorides are given in Table 2. The results are in reasonably good agreement with the value presiously measured by Dennison in this laboratory.

No thermal arrests were detected for the orthorhombic to hexagonal transition in LaF_3, CeF_3, PrF_3, NdF_3, EuF_3, TbF_3, DyF_3 and HoF_3. The orthorhombic to hexagonal transition has never been detected for LaF_3 through NdF_3. However, Thoma and Brunton (33) have determined the transition temperatures of EuF_3, TbF_3, DyF_3 and HoF_3 by high temperature x-ray diffraction techniques. Figure 6 shows the dimorphism exhibited by the rare earth fluorides.

Although the lattice parameters of the rare earth trifluorides have previously been measured by several people,

Table 2. The transition temperatures, melting points, heats of transformation, entropies of transformation, heats of fusion, and entropies of fusion of the rare earth trifluorides

Salt	Transition Temperature (Deg. C.)	Melting Point (Deg. C.)	ΔH_{tr} $\left(\frac{cal}{mole}\right)$	ΔS_{tr} $\left(\frac{cal}{mole\ deg}\right)$	ΔH_{fus} $\left(\frac{cal}{mole}\right)$	ΔS_{fus} $\left(\frac{cal}{mole\ deg}\right)$
YF_3	1077±3	1155±3	7750	5.74	6685	4.68
LaF_3		1493±3			12009	6.80
CeF_3		1430±3			13200[a]	7.62[a]
PrF_3		1399±3			13699	8.19
NdF_3		1377±3			13075	7.92
SmF_3	489±3	1298±3				
EuF_3	700[b]	1276±3				
GdF_3	1074±3	1230±3	307	0.23	12041	8.01
TbF_3	950±6[b]	1173±3				
DyF_3	1030±6[b]	1155±3				

[a]King and Christensen (56).

[b]Thoma and Brunton (33).

Table 2 (continued)

Salt	Transition Temperature (Deg. C.)	Melting Point (Deg. C.)	ΔH_{tr} $\left(\frac{cal}{mole}\right)$	ΔS_{tr} $\left(\frac{cal}{mole\ deg}\right)$	ΔH_{fus} $\left(\frac{cal}{mole}\right)$	ΔS_{fus} $\left(\frac{cal}{mole\ deg}\right)$
HoF_3	1070±6[a]	1143±3			13459	9.50
ErF_3	1115±3	1144±3				
TmF_3	1052±3	1156±3				
YbF_3	994±3	1170±3				
LuF_3	957±3	1184±3	5986	4.87	7231	4.96

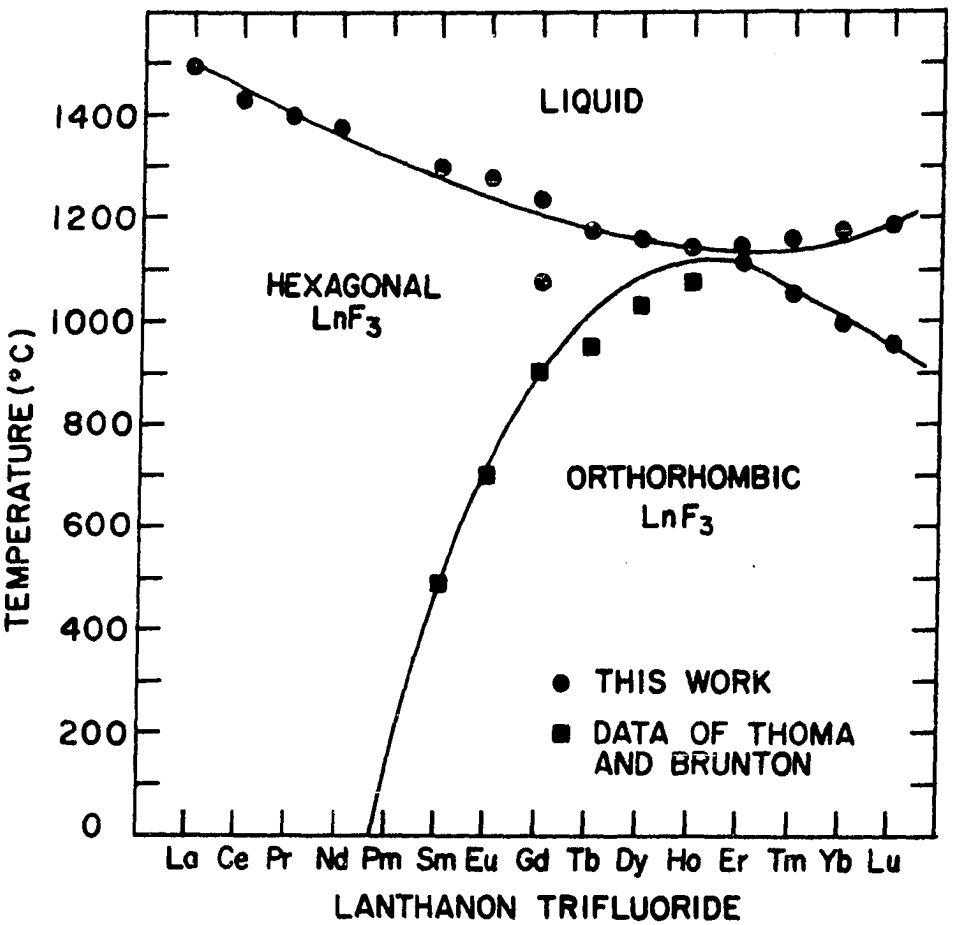

Figure 6. The equilibrium dimorphism of the rare earth trifluorides

the determination of the lattice parameters for the purer materials of this work would serve as a check on the effect of purity on the size of the unit cell. The lattice parameters of the rare earth trifluorides were determined using the Debye-Scherrer powder technique. The samples for the x-ray work were prepared by grinding the fluorides to a very fine powder in an inert atmosphere (argon) and then loading the powder into 0.3 mm. capillary tubes. At least two patterns of each fluoride using different samples were taken using a standard Debye-Scherrer powder camera and filtered chromium Kα radiation.

The patterns were indexed with the aid of a computer program (74) which generated hkl and $\sin^2\theta$ values from lattice parameter data. The precision lattice parameters were then determined by extrapolation of the data to $\theta = 90^{\circ}$ with a Vogel-Kempter computer program (75) which uses a Nelson Riley extrapolation function. The lattice parameters reported in this work are an average of at least two patterns of different samples. The values of the different determinations for each fluoride agree within the calculated standard deviation which was less than ± 0.001 Å. A summary of the results of the powder data is given in Table 3. The observed $\sin^2\theta$ and hkl values from the powder work are given in Appendix B. The lattice parameters determined in this work are in reasonable agreement with previous values.

Table 3. The room temperature lattice parameters of the rare earth trifluorides

Salt	Symmetry	Space Group	Lattice Parameters a	b	c	Calculated Density (gms/cc)
YF_3	Orthorhombic	Pnma	6.367	6.859	4.394	5.048
LaF_3	Trigonal	$P\bar{3}c1$	7.186		7.352	5.935
CeF_3	Trigonal	$P\bar{3}c1$	7.112		7.279	6.158
PrF_3	Trigonal	$P\bar{3}c1$	7.078		7.239	6.277
NdF_3	Trigonal	$P\bar{3}c1$	7.030		7.200	6.505
SmF_3	Orthorhombic	Pnma	6.674	7.059	4.404	6.636
EuF_3[a]	Orthorhombic	Pnma	6.622	7.019	4.396	6.791
GdF_3	Orthorhombic	Pnma	6.575	6.985	4.391	7.055
TbF_3	Orthorhombic	Pnma	6.510	6.947	4.386	7.229
DyF_3	Orthorhombic	Pnma	6.460	6.906	4.376	7.466
HoF_3	Orthorhombic	Pnma	6.405	6.874	4.378	7.646
ErF_3	Orthorhombic	Pnma	6.350	6.844	4.383	7.818
TmF_3	Orthorhombic	Pnma	6.278	6.813	4.410	7.954

[a]Thoma and Brunton (33).

Table 3 (continued)

Salt	Symmetry	Space Group	Lattice Parameters a	b	c	Calculated Density (gms/cc)
Yb_3	Orthorhombic	Pnma	6.217	6.787	4.433	8.167
LuF_3	Orthorhombic	Pnma	6.145	6.761	4.472	8.291

Thermodynamic Properties

Aluminum oxide

As a check of the accuracy of the calorimeter, the heat content of α-Al_2O_3 was determined over the temperature range of 400 to 1400°K. Measurements were made at one hundred degree intervals and the heat content was taken to be the average of a series of measurements involving three samples of different weights. A comparison of the values obtained in this work and the National Bureau of Standards data of Furukawa *et al.* (73) is shown in Figure 7. This work agrees with their values within ± 0.5%.

Rare earth fluorides

The heat contents of YF_3, LaF_3, PrF_3, NdF_3, GdF_3, HoF_3 and LuF_3 were determined over a temperature range of 100 to 1600°C. (373 to 1873°K.). The data were taken at approximately fifty degree intervals except in the vicinity of the transition temperatures and the melting points where measurements were made at smaller intervals. A minimum of two samples of different weights were used for each temperature range to check the precision of the equipment.

The heat contents were calculated from the raw data and corrected to the standard reference temperature of 298.16°K. as described previously. The plots of the heat content, $H_T^o - H_{298}^o$, versus temperature are shown in Figures 8-14. There is only one discontinuity in the heat content curves for

LaF_3, PrF_3 and NdF_3. This corresponds to the trigonal (solid)-liquid transition. There are two discontinuities in the heat content curves for YF_3, GdF_3 and LuF_3. These correspond to the orthorhombic-hexagonal (trigonal) solid phase transition and the hexagonal (trigonal)-liquid transition. In the case of HoF_3 there is only one actual discontinuity in the heat content curve which corresponds to the hexagonal (trigonal)-liquid transition. However, there is a change in slope in the heat content curve occurring at $1343^{\circ}K$. This is believed to be the orthorhombic-hexagonal (trigonal) phase transition that has been observed by high temperature x-ray diffraction.

An empirical equation was determined by a least squares technique to represent each region of the heat content curves for each salt. In all regions, the data were fitted to the equation suggested by Maier and Kelley (72). The empirical equations, the temperature range over which they apply, and the standard deviation of the values calculated from the empirical equations from the observed values are given at the end of Tables 4-10.

The latent heat of transition and the latent heat of fusion were calculated for each salt. The latent heats were found by calculating the heat contents at the transition temperature from the empirical equations for the curves above and below the transition and subtracting the lower value from the higher value. The corresponding entropies were calculated

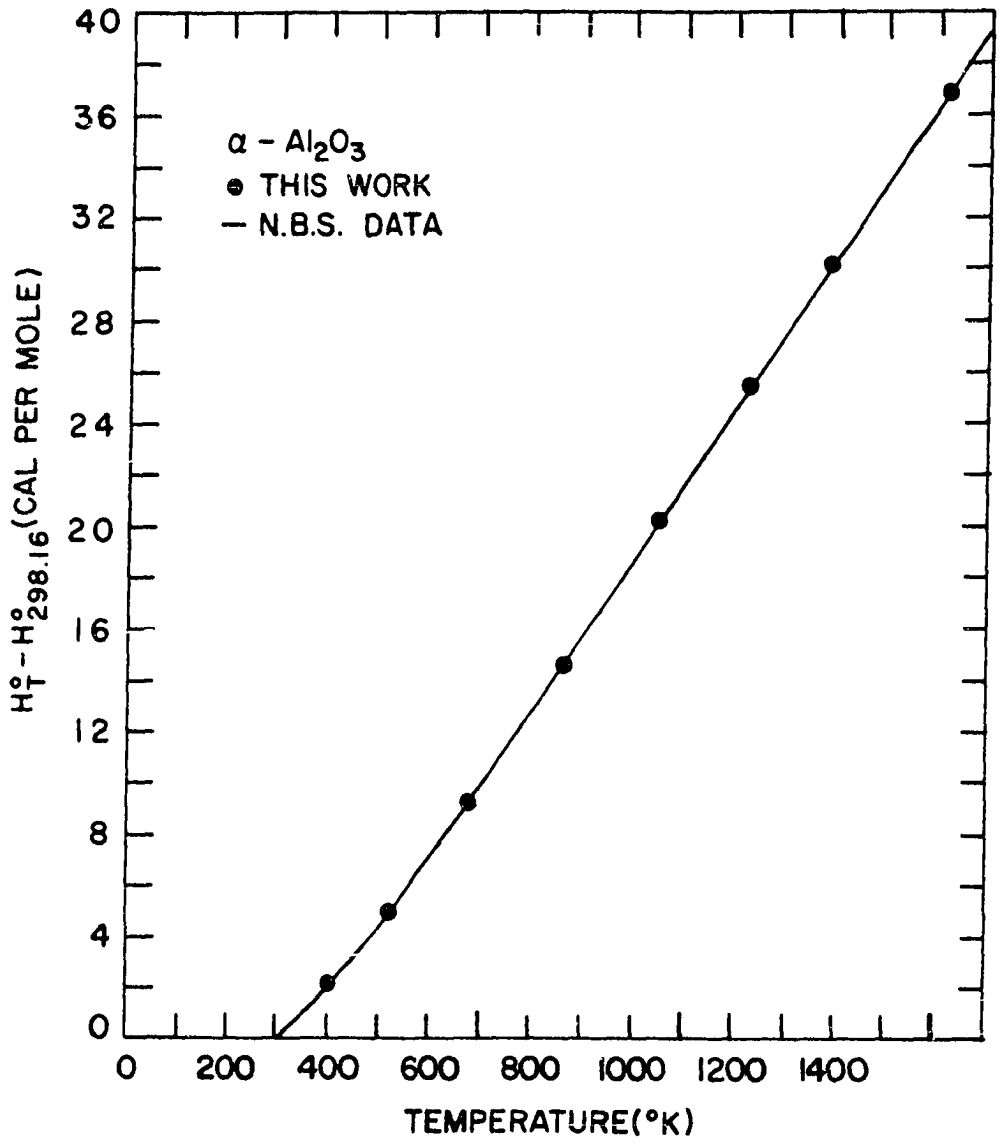

Figure 7. The measured enthalpy of α-Al_2O_3

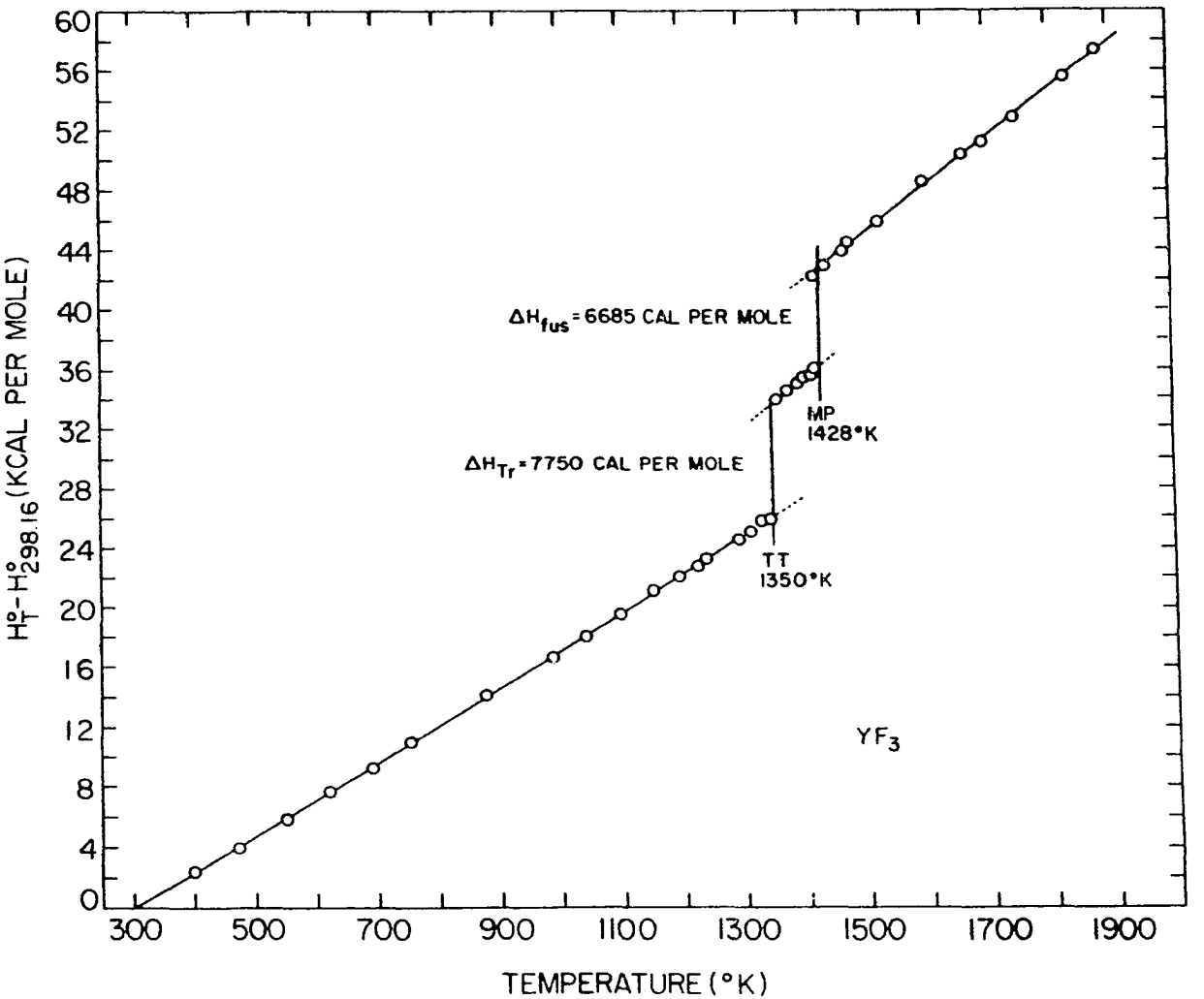

Figure 8. The measured enthalpy of YF_3

Table 4. Thermodynamic functions for YF_3

$T^{\circ}K.$	$H_T^{\circ} - H_{298}^{\circ}$ [a]	C_p [b]	$S_T^{\circ} - S_{298}^{\circ}$ [b]	$-\left(\frac{F_T^{\circ} - H_{298}^{\circ}}{T}\right)$ [b]
373	1632	23.45	5.19	28.31
423	2813	23.75	8.16	29.01
473	4006	23.99	10.83	29.86
523	5211	24.19	13.25	30.78
573	6425	24.36	15.46	31.75
623	7648	24.52	17.51	32.74
673	8877	24.66	19.41	33.72
723	10113	24.78	21.18	34.69
773	11355	24.91	22.84	35.65
823	12604	25.02	24.41	36.59
873	13858	25.13	25.88	37.51
923	15117	25.24	27.29	38.41
973	16382	25.34	28.62	39.29
1023	17651	25.45	29.90	40.14
1073	18926	25.55	31.11	40.97
1123	20206	25.65	32.28	41.78
1173	21491	25.74	33.40	42.58
1223	22781	25.84	34.47	43.35
1273	24075	25.94	35.51	44.10
1323	25375	26.03	36.51	44.83
1350	26078	26.08	37.04	45.22
1350	33828	29.24	42.78	45.22
1363	34208	29.21	43.06	45.46
1383	34792	29.19	43.48	45.83
1403	35376	29.21	43.90	46.19
1423	35961	29.27	44.32	46.55
1428	36107	29.29	44.42	46.64
1428	42792	31.95	49.10	46.64
1433	42952	31.95	49.21	46.74
1473	44230	31.95	50.09	47.57
1523	45827	31.95	51.16	48.57
1573	47424	31.95	52.19	49.54
1623	49022	31.95	53.19	50.49
1673	50619	31.95	54.16	51.40
1723	52217	31.95	55.10	52.30
1773	53814	31.95	56.01	53.16
1823	55411	31.95	56.90	54.01
1873	57009	31.95	57.77	54.83

[a] cal/mole.

[b] cal/mole deg.

Table 4 (continued)

Transition temperature: 1350°K.

Melting point: 1428°K.

Latent heat of transition: 7750 ± 100 cal/mole

Entropy of transition: 5.74 ± 0.1 cal/mole deg

Latent heat of fusion: 6685 ± 100 cal/mole

Entropy of fusion: 4.68 ± 0.1 cal/mole deg

$H_T^o - H_{298.16}^o = -7718.7 + 23.762T + 0.00088764T^2 + 135843T^{-1}$ [c] (373 < T < 1350°K.)

$H_T^o - H_{298.16}^o = 140455 - 76.353T + 0.025426T^2 - 6.7350 \times 10^7 T^{-1}$ [d] (1350 < T < 1428°K.)

$H_T^o - H_{298.16}^0 = -2852.2 + 31.962T - 3.0818 \times 10^{-6} T^2 + 11500T^{-1}$ [d] (1428 < T < 1873°K.)

$S_{298.16}^o = 27.5$ cal/mole deg

[c] Standard deviation is ± 0.75%.

[d] Standard deviation is ± 1.0%.

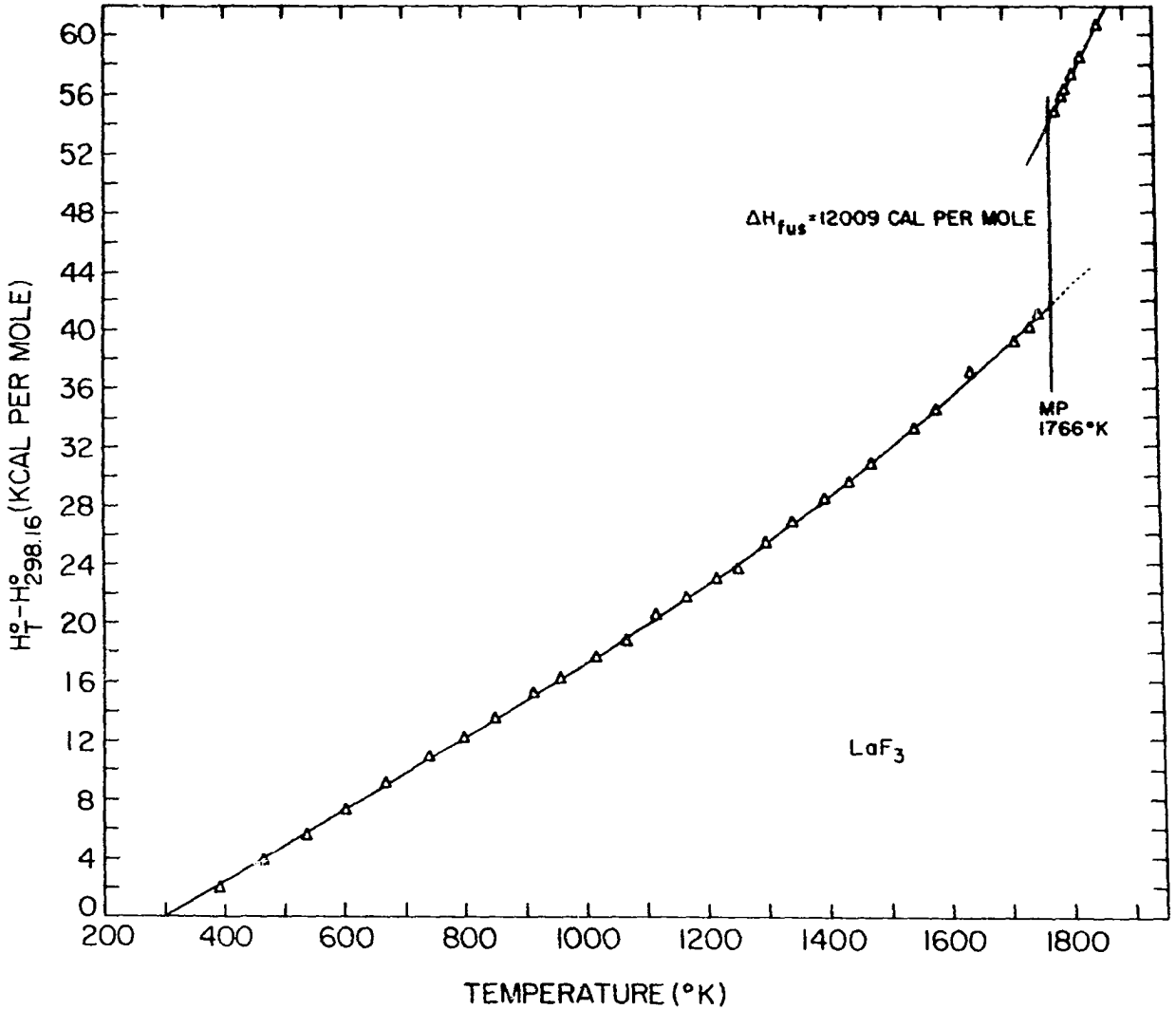

Figure 9. The measured enthalpy of LaF_3

Table 5. Thermodynamic functions for LaF_3

$T^oK.$	$H_T^o - H_{298}^o$ [a]	C_p [b]	$S_T^o - S_{298}^o$ [b]	$-\left(\frac{F_T^o - H_{298}^o}{T}\right)$ [b]
373	1789	24.14	5.38	28.08
423	3000	24.29	8.43	28.84
473	4218	24.42	11.15	29.73
523	5441	24.52	13.61	30.70
573	6669	24.61	15.85	31.71
623	7902	24.68	17.91	32.73
673	9138	24.75	19.82	33.74
723	10377	24.82	21.60	34.74
773	11617	24.88	23.26	35.73
823	12864	24.94	24.82	26.69
873	14113	24.99	26.29	37.92
923	15364	25.04	27.68	38.54
973	16615	25.11	29.01	39.43
1023	17878	25.46	30.27	40.30
1073	19163	25.95	31.50	41.14
1123	20475	26.55	32.69	41.96
1173	21820	27.25	33.86	42.76
1223	23201	28.03	35.02	43.55
1273	24624	28.88	36.16	44.32
1323	26090	29.79	37.29	45.07
1373	27604	30.74	38.41	45.81
1423	29166	31.74	39.53	46.53
1473	30779	32.78	40.64	47.25
1523	32444	33.85	41.75	47.95
1573	34164	34.95	42.86	48.65
1623	35940	36.08	43.98	49.33
1673	37772	37.22	45.09	50.01
1723	39662	38.39	46.20	50.68
1766	41325	39.40	47.16	51.25
1766	53334	80.82	53.96	51.25
1773	53909	80.73	54.28	51.37
1823	57948	80.80	56.53	52.24
1863	61179	80.76	58.28	52.94

[a] cal/mole.

[b] cal/mole deg.

Table 5 (continued)

Melting point: 1766°K.

Latent heat of fusion: 12009 ± 100 cal/mole

Entropy of fusion: 6.80 ± 0.1 cal/mole deg

$H_T^\circ - H_{298.16}^\circ = -7534.1 + 24.322T + 0.0004359T^2 + 70828T^{-1}$ [c] (373 < T < 950°K.)

$H_T^\circ - H_{298.16}^\circ = 26120 - 12.374T + 0.013734T^2 - 1.0187 \times 10^7 T^{-1}$ [c] (950 < T < 1766°K.)

$H_T^\circ - H_{298.16}^\circ = -258623 + 173.68T - 0.016987T^2 + 1.0284 \times 10^8 T^{-1}$ [d] (1766 < T < 1873°K.)

$S_{298.16}^\circ = 27.5$ cal/mole deg

[c] Standard deviation is ± 0.70%.

[d] Standard deviation is ± 1.0%.

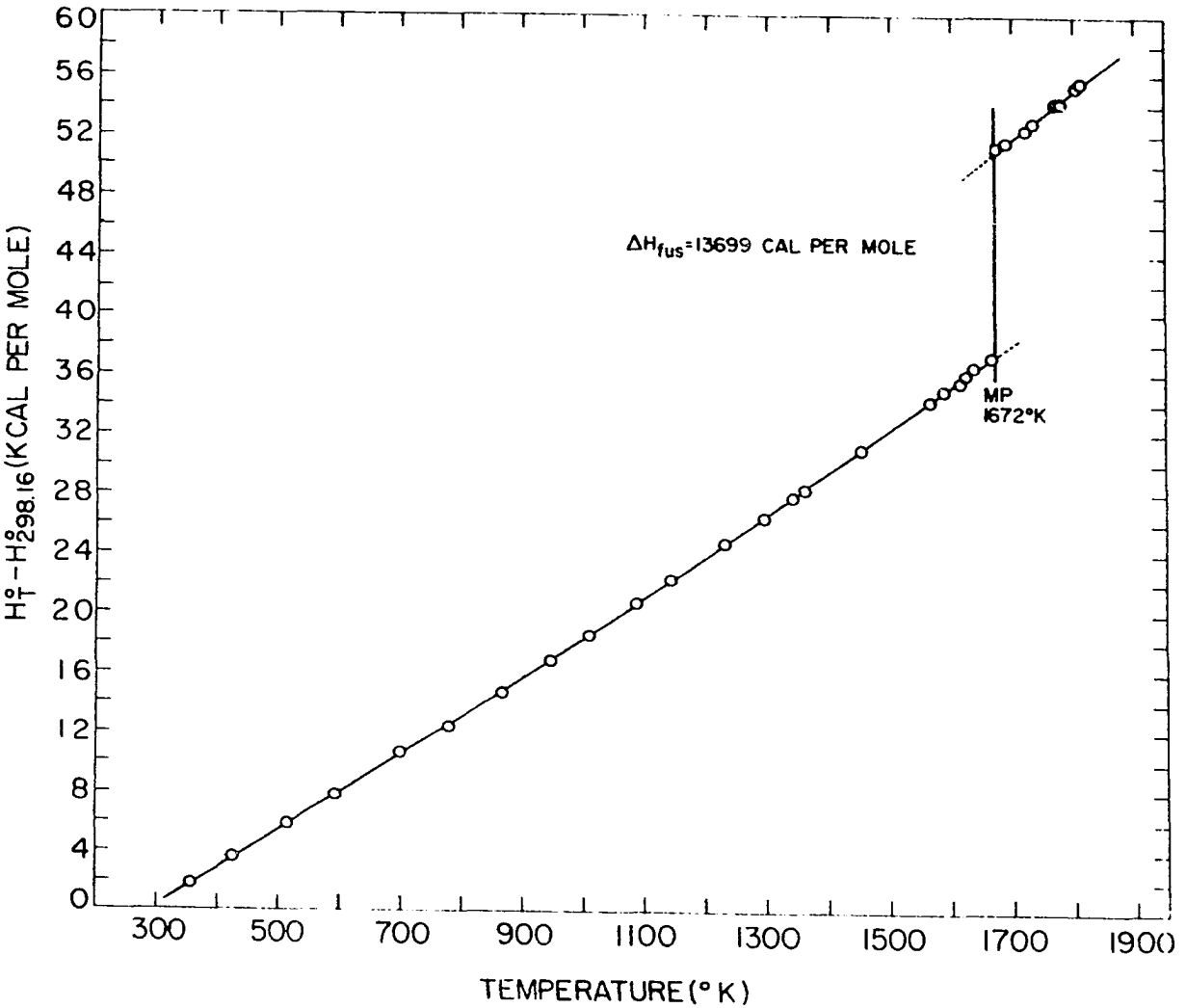

Figure 10. The measured enthalpy of PrF_3

Table 6. Thermodynamic functions for PrF_3

$T^{o}K.$	$H_T^o - H_{298}^o$ [a]	C_p [b]	$S_T^o - S_{298}^o$ [b]	$-\left(\frac{F_T^o - H_{298}^o}{T}\right)$ [b]
373	2138	25.05	5.66	27.43
423	3388	24.98	8.81	28.30
473	4638	25.00	11.60	29.30
523	5889	25.08	14.12	30.36
573	7147	25.20	16.41	31.44
623	8410	25.36	18.53	32.53
673	9682	25.53	20.49	33.60
723	10963	25.71	22.33	34.66
773	12254	25.91	24.05	35.70
823	13554	26.11	25.68	36.71
873	14865	26.32	27.23	37.70
923	16817	26.54	28.70	38.66
973	17519	26.76	30.11	39.60
1023	18863	26.98	31.46	40.52
1073	20218	27.21	32.75	41.41
1123	21584	27.44	33.99	42.27
1173	22962	27.67	35.19	43.12
1223	24351	27.90	36.35	43.94
1273	25752	28.14	37.48	44.75
1323	27165	28.37	38.56	45.53
1373	28589	28.61	39.62	46.30
1423	30025	28.84	40.65	47.05
1473	31473	29.08	41.65	47.78
1523	32933	29.32	42.62	48.50
1573	34405	29.56	43.57	49.20
1623	35889	29.80	44.50	49.89
1672	37355	30.02	45.40	50.56
1672	51054	31.25	53.59	50.56
1723	52648	31.25	54.52	51.47
1773	54210	31.25	55.42	52.34
1823	55773	31.26	56.29	53.19
1863	57024	31.26	56.97	53.86

[a] cal/mole.

[b] cal/mole deg.

Table 6 (continued)

Melting point: 1672°K.

Latent heat of fusion: 13699 ± 100 cal/mole

Entropy of fusion: 8.19 ± 0.1 cal/mole deg

$H_T^o - H_{298.16}^o = -5801.8 + 21.806T + 0.0024379T^2 - 1.9885 \times 10^5 T^{-1}$ [c] (373 < T < 1672°K.)

$H_T^o - H_{298.16}^o = 3299.0 + 28.649T + 5.0205 \times 10^{-4} T^2 - 2.5907 \times 10^6 T^{-1}$ [d] (1672 < T < 1863°K.)

$S_{298.16}^o = 27.5$ cal/mole

[c] Standard deviation is ± 0.75%.

[d] Standard deviation is ± 1.0%.

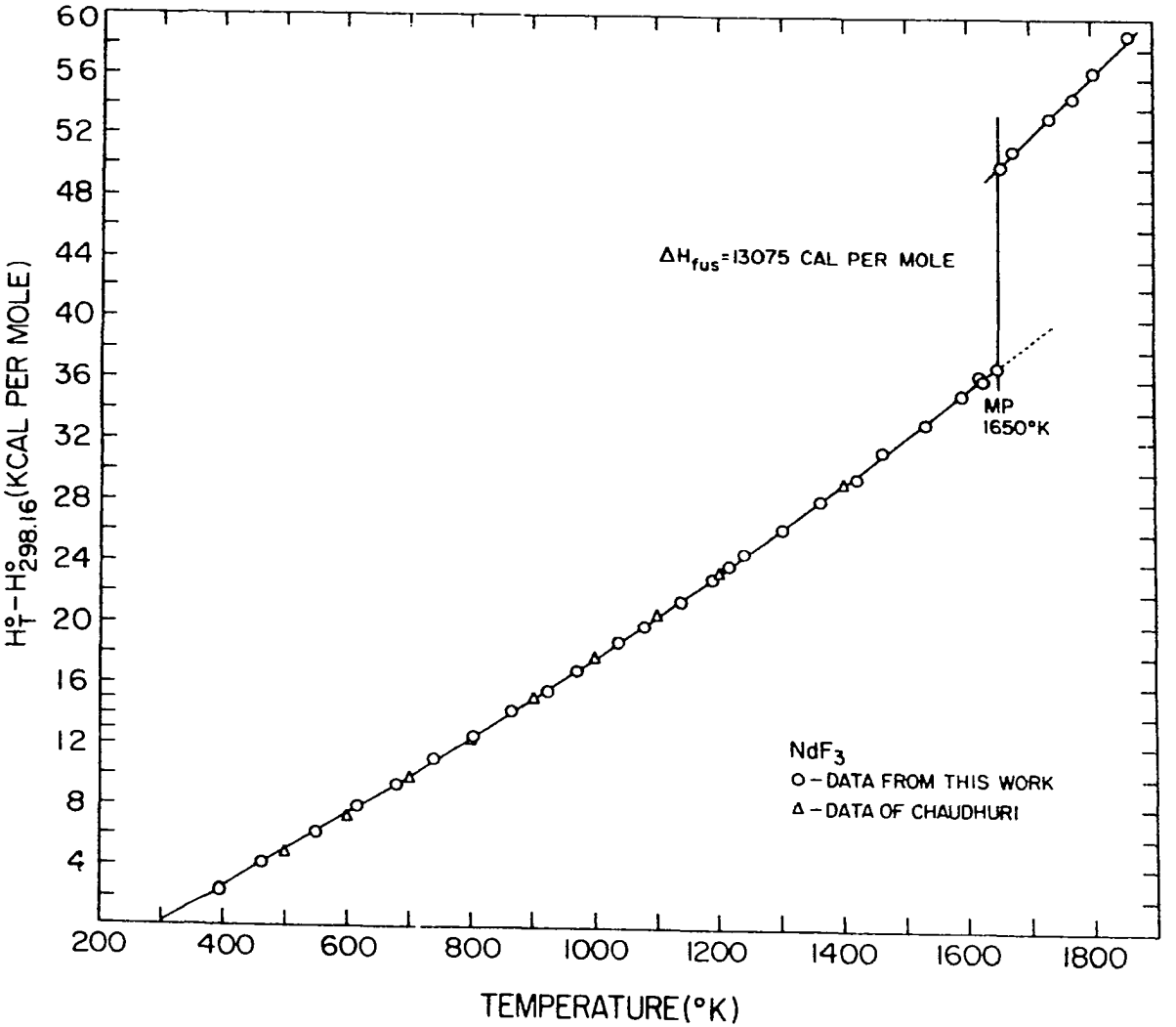

Figure 11. The measured enthalpy of NdF_3

Table 7. Thermodynamic functions for NdF_3

$T^oK.$	$H_T^o - H_{298}^o$ [a]	C_p [b]	$S_T^o - S_{298}^o$ [b]	$-\left(\frac{F_T^o - H_{298}^o}{T}\right)$ [b]
373	1855	24.63	5.66	28.18
423	3077	24.29	8.73	28.96
473	4288	24.18	11.44	29.87
523	5498	24.21	13.87	30.86
573	6712	24.35	16.08	31.87
623	7934	24.56	18.13	32.90
673	9168	24.81	20.04	33.91
723	10416	25.10	21.82	34.92
773	11679	25.42	23.51	35.90
823	12959	25.76	25.12	36.87
873	14255	26.11	26.65	37.82
923	15570	26.48	28.11	38.74
973	16903	26.85	29.51	39.65
1023	18255	27.24	30.87	40.53
1073	19627	27.63	32.18	41.39
1123	21018	28.02	33.45	42.23
1173	22430	28.42	34.68	43.06
1223	23861	28.83	35.87	43.86
1273	25313	29.24	37.04	44.65
1323	26785	29.65	38.17	45.43
1373	28277	30.06	39.28	46.18
1423	29791	30.47	40.36	46.93
1473	31325	30.89	41.42	47.66
1523	32880	31.31	42.46	48.37
1573	34456	31.73	43.48	49.07
1623	36053	32.15	44.48	49.76
1650	36924	32.42	45.01	50.13
1650	49999	41.29	52.93	50.13
1673	50949	41.30	53.50	50.55
1723	53014	41.30	54.72	51.45
1773	55079	41.30	55.90	52.34
1823	57145	41.30	57.05	53.20
1873	59210	41.29	58.17	54.06

[a] cal/mole.

[b] cal/mole deg.

Table 7 (continued)

Melting point: 1650°K.

Latent heat of fusion: 13075 ± 100 cal/mole

Entropy of fusion: 7.92 ± 0.1 cal/mole deg

$H_T^o - H_{298.16}^o = -4130.7 + 17.918T + 0.0043283T^2 - 4.8471 \times 10^5 T^{-1}$ [c] (373 < T < 1650°K.)

$H_T^o - H_{298.16}^o = -23032 + 44.087T - 0.00052869T^2 + 2.84965 \times 10^6 T^{-1}$ [d] (1650 < T < 1873°K.)

$S_{298.16}^o = 27.5$ cal/mole deg

[c] Standard deviation is ± 0.75%.

[d] Standard deviation is ± 1.0%.

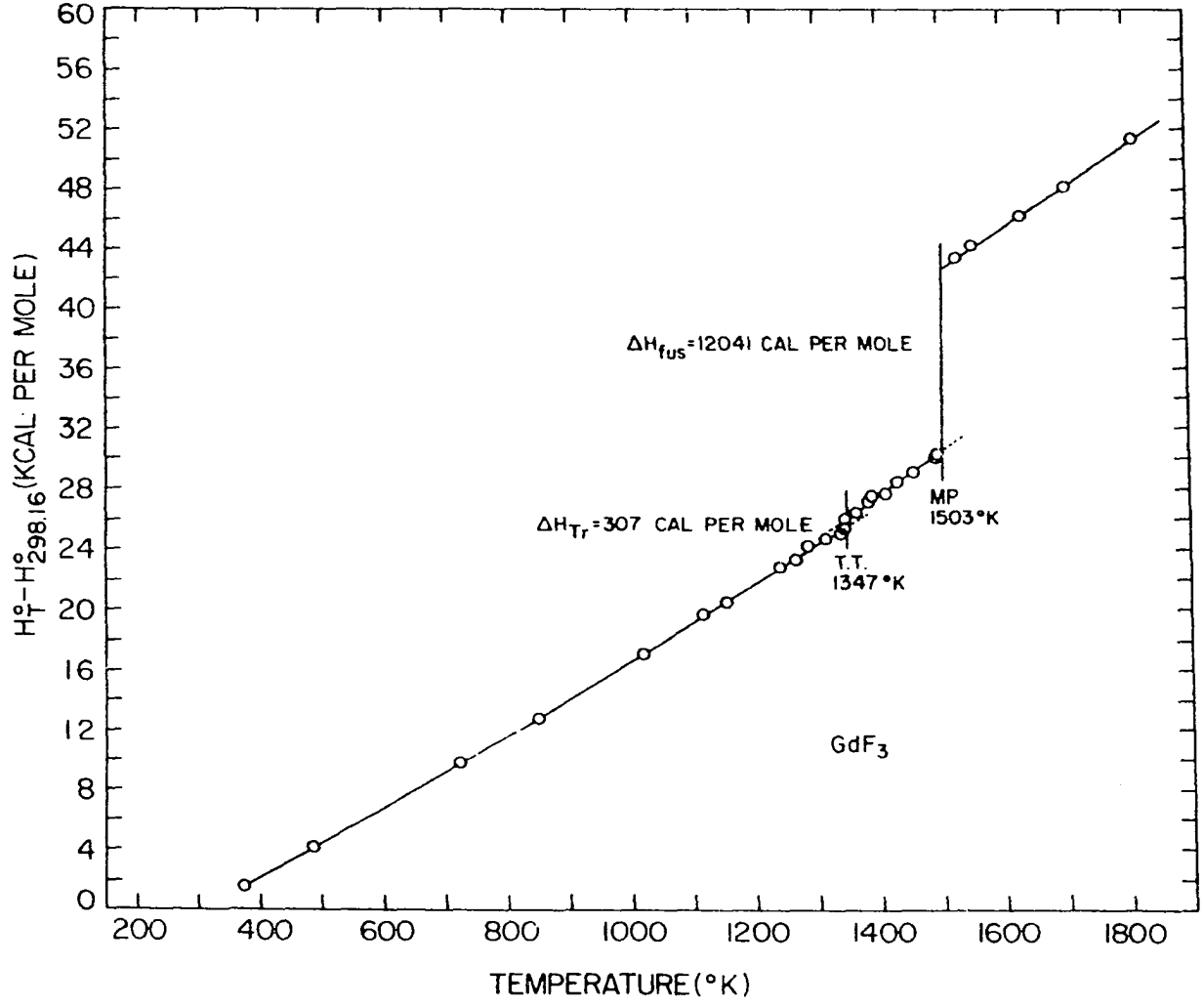

Figure 12. The measured enthalpy of GdF_3

Table 8. Thermodynamic functions for GdF_3

$T^oK.$	$H_T^o - H_{298}^o$ [a]	C_p [b]	$S_T^o - S_{298}^o$ [b]	$-\left(\frac{F_T^o - H_{298}^o}{T}\right)$ [b]
373	1552	22.32	4.96	28.30
423	2675	22.60	7.79	28.96
473	3812	22.87	10.32	29.77
523	4962	23.13	12.64	30.65
573	6125	23.39	14.76	31.57
623	7301	23.64	16.73	32.51
673	8489	23.89	18.56	33.45
723	9690	24.14	20.28	34.38
773	10903	24.39	21.90	35.30
823	12129	24.63	23.44	36.20
873	13368	24.89	24.90	37.09
923	14619	25.14	26.30	37.96
973	15882	25.39	27.63	38.81
1023	17157	25.64	28.91	39.64
1073	18445	25.88	30.14	40.45
1123	19746	26.13	31.32	41.24
1173	21058	26.38	32.46	42.01
1223	22383	26.62	33.57	42.77
1273	23721	26.87	34.64	43.51
1323	25070	27.12	35.68	44.23
1347	25722	27.23	36.16	44.58
1347	26029	28.89	36.39	44.58
1373	26776	28.46	36.95	44.95
1423	28190	28.28	37.96	45.65
1473	29622	29.17	38.95	46.34
1503	30511	29.88	39.58	46.78
1503	42552	27.97	47.59	46.78
1523	43111	27.97	47.96	47.15
1573	44510	27.98	48.86	48.06
1623	45909	27.98	49.74	48.95
1673	47308	27.98	50.58	49.81
1723	48706	27.97	51.41	50.64
1773	50105	27.97	52.21	51.45
1823	51504	27.97	52.99	52.24
1863	52622	27.97	53.59	52.85

[a] cal/mole.

[b] cal/mole deg.

Table 8 (continued)

Transition temperature: 1347°K.

Melting point: 1503°K.

Latent heat of transition: 307 ± 100 cal/mole

Entropy of transition: 0.23 ± 0.1 cal/mole deg

Latent heat of fusion: 12041 ± 100 cal/mole

Entropy of fusion: 8.01 ± 0.1 cal/mole deg

$H_T^o - H_{298.16}^o = -6537.2 + 20.633T + 0.0024541T^2 + 19298T^{-1}$ [c] (373 < T < 1347°K.)

$H_T^o - H_{298.16}^o = 602471 - 408.98T + 0.10370T^2 - 2.87842 \times 10^8 T^{-1}$ [c] (1347 < T < 1503°K.)

$H_T^o - H_{298.16}^o = -336.32 + 28.494T - 0.00010633T^2 + 45349T^{-1}$ [d] (1503 < T < 1863°K.)

$S_{298.16}^o = 27.5$ cal/mole deg

[c] Standard deviation is ± 0.75%.

[d] Standard deviation is ± 1.0%.

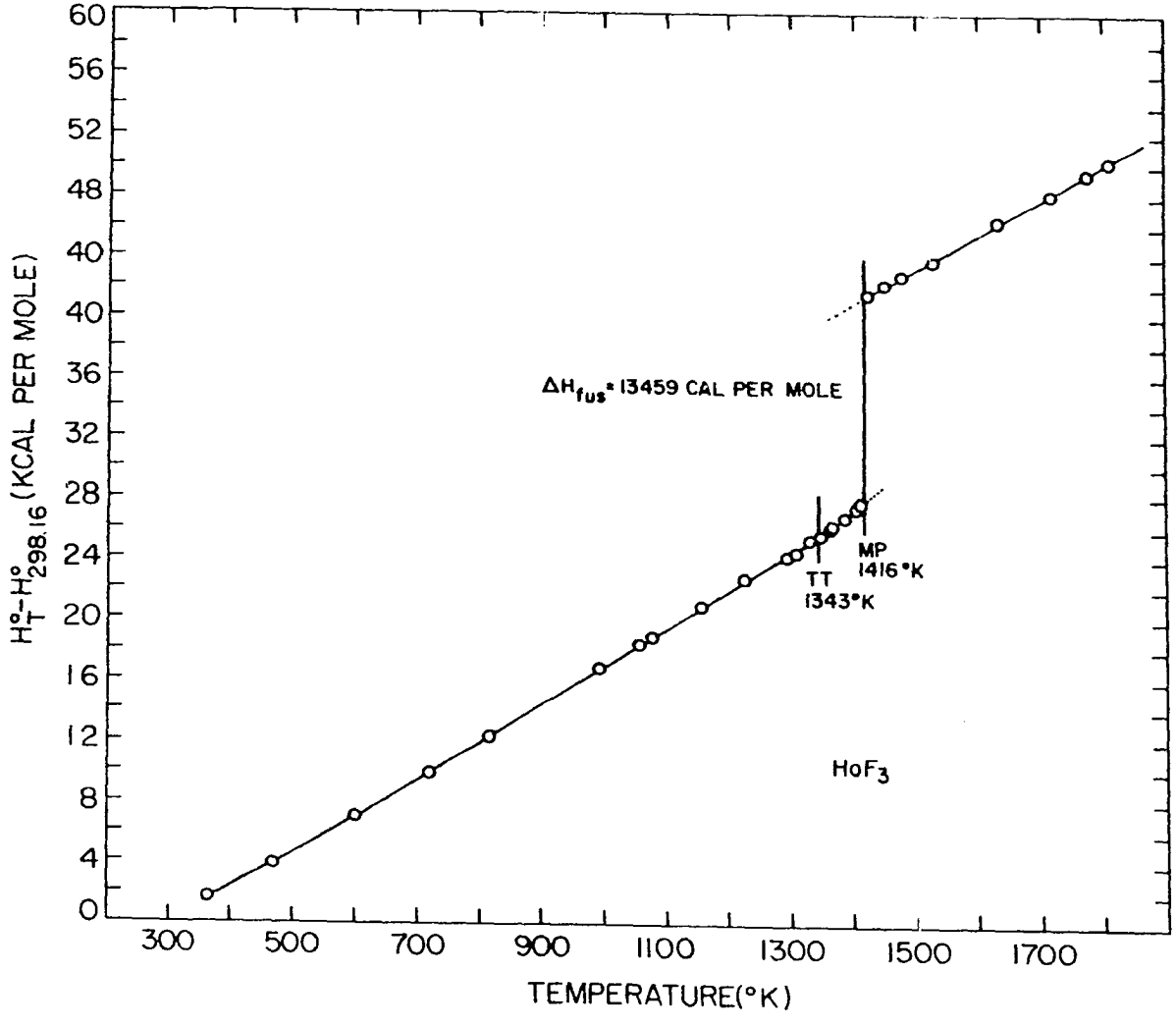

Figure 13. The measured enthalpy of HoF_3

Table 9. Thermodynamic functions for HoF_3

$T^oK.$	$H_T^o - H_{298}^o$ [a]	C_p [b]	$S_T^o - S_{298}^o$ [b]	$-\frac{(F_T^o - H_{298}^o)}{T}$ [b]
373	1690	21.96	4.72	27.69
423	2809	22.78	7.53	28.39
473	3963	23.34	10.11	29.23
523	5141	23.76	12.48	30.15
573	6337	24.07	14.66	31.10
623	7548	24.32	16.69	32.07
673	8768	24.51	18.57	33.04
723	9998	24.66	20.33	34.00
773	11234	24.79	21.99	34.95
823	12476	24.89	23.54	35.88
873	13723	24.98	25.01	36.79
923	14974	25.06	26.41	37.68
973	16229	25.12	27.73	38.55
1023	17486	25.18	28.99	39.40
1073	18747	25.23	30.19	40.22
1123	20009	25.27	31.34	41.03
1173	21274	25.31	32.45	41.81
1223	22540	25.35	33.50	42.57
1273	23809	25.38	34.52	43.32
1323	25078	25.41	35.50	44.04
1343	25586	25.42	35.88	44.33
1343	25530	30.93	35.84	44.33
1373	26458	30.93	36.52	44.75
1416	27788	30.93	37.48	45.35
1416	41247	22.94	46.98	45.35
1423	41407	22.94	47.09	45.49
1473	42555	22.94	47.88	46.50
1523	43702	22.94	48.65	47.46
1573	44849	22.94	49.39	48.38
1623	45996	22.94	50.11	49.27
1673	47143	22.94	50.80	50.13
1723	48290	22.94	51.48	50.95
1773	49437	22.94	52.14	51.75
1823	50584	22.94	52.78	52.53
1843	51043	22.94	53.03	52.83

[a] cal/mole.

[b] cal/mole deg.

Table 9 (continued)

Transition temperature: $1343^{\circ}K.$

Melting point: $1416^{\circ}K.$

Latent heat of transition: not observable within experimental error

Latent heat of fusion: 13459 ± 100 cal/mole

Entropy of fusion: 9.50 ± 0.1 cal/mole deg

$$H_T^{\circ} - H_{298.16}^{\circ} = -9197.5 + 25.544T + 5.7461 \times 10^{-5}T^2 + 5.0401 \times 10^{5}T^{-1}\ ^{c} \quad (373 < T < 1343^{\circ}K.)$$

$$H_T^{\circ} - H_{298.16}^{\circ} = 27169 + 39.045T - 0.0019663T^2 + 5.11358 \times 10^{6}T^{-1}\ ^{c} \quad (1343 < T < 1416^{\circ}K.)$$

$$H_T^{\circ} - H_{298.16}^{\circ} = 8917.2 + 22.846T + 1.9489 \times 10^{-5}T^2 - 85094T^{-1}\ ^{d} \quad (1416 < T < 1843^{\circ}K.)$$

$$S_{298.16}^{\circ} = 27.5 \text{ cal/mole deg}$$

[c] Standard deviation is ± 0.70%.

[d] Standard deviation is ± 1.0%.

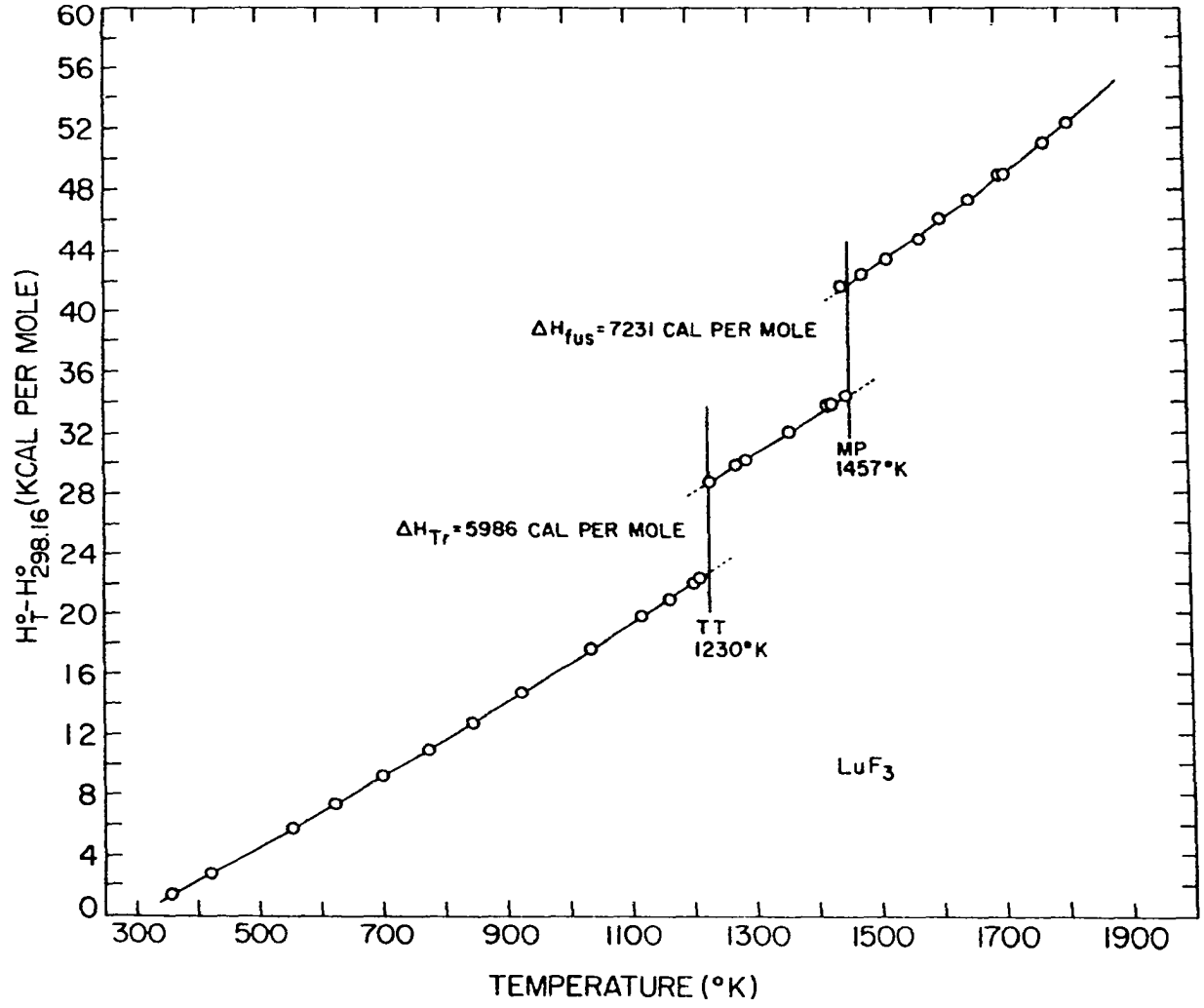

Figure 14. The measured enthalpy of LuF_3

Table 10. Thermodynamic functions for LuF_3

$T^oK.$	$H_T^o - H_{298}^o$ [a]	C_p [b]	$S_T^o - S_{298}^o$ [b]	$-\left(\frac{F_T^o - H_{298}^o}{T}\right)$ [b]
373	1625	21.81	4.80	27.94
423	2727	22.26	7.57	28.63
473	3850	22.65	10.08	29.44
523	4991	23.00	12.38	30.33
573	6149	23.33	14.49	31.26
623	7324	23.64	16.46	32.20
673	8513	23.94	18.29	33.14
723	9718	24.23	20.02	24.08
773	10936	24.51	21.65	35.00
823	12169	24.79	23.19	35.91
873	13415	25.06	24.66	36.80
923	14675	25.33	26.06	37.67
973	15948	25.60	27.41	38.52
1023	17235	25.87	28.70	39.35
1073	18535	26.13	29.94	40.16
1123	19848	26.39	31.14	40.96
1173	21174	26.66	32.29	41.74
1223	22514	26.92	33.41	42.50
1230	22702	26.96	33.56	42.60
1230	28688	25.44	38.43	42.60
1273	29782	25.44	39.30	43.41
1323	31054	25.44	40.28	44.31
1373	32326	25.44	41.23	45.18
1423	33598	25.44	42.14	46.03
1457	34462	25.44	42.74	46.58
1457	41693	24.90	47.70	46.58
1473	42092	25.18	47.97	46.90
1523	43397	26.95	48.84	47.85
1573	44784	28.51	49.74	48.77
1623	46245	29.90	50.65	49.66
1673	47771	31.13	51.58	50.52
1723	49356	32.22	52.51	51.37
1773	50992	33.19	53.45	52.19
1823	52673	34.05	54.38	52.99
1873	54395	34.82	55.32	53.77

[a] cal/mole.

[b] cal/mole deg.

Table 10 (continued)

Transition temperature: 1230°K.

Melting point: 1457°K.

Latent heat of transition: 5986 ± 100 cal/mole

Entropy of transition: 4.87 ± 0.1 cal/mole deg

Latent heat of fusion: 7231 ± 100 cal/mole

Entropy of fusion: 4.96 ± 0.1 cal/mole deg

$H_T^\circ - H_{298.16}^\circ = -6812.0 + 20.796T + 0.0025351T^2 + 1.2188 \times 10^5 T^{-1}$ [c] $(373 < T < 1230^\circ K.)$

$H_T^\circ - H_{298.16}^\circ = -2107.6 + 25.064T + 9.5141 \times 10^{-5} T^2 - 2.1725 \times 10^5 T^{-1}$ [c] $(1230 < T < 1457^\circ K.)$

$H_T^\circ - H_{298.16}^\circ = -1.0127 \times 10^5 + 69.689T - 0.0038178T^2 + 7.2167 \times 10^7 T^{-1}$ [d] $(1457 < T < 1873^\circ K.)$

$S_{298.16}^\circ = 27.5$ cal/mole deg

[c] Standard deviation is ± 0.75%.

[d] Standard deviation is ± 1.0%.

by dividing the latent heat by the transition temperature. The results of these calculations for each salt are given in Tables 4-10 and are compiled in Table 1.

The thermodynamic functions for the rare earth fluorides were calculated using equations 20, 21 and 23. Since sufficient data to evaluate S^{o}_{298} for the fluorides were not available, it was necessary to estimate this value in order to calculate the free energy functions. Westrum and Beale (57) have determined the low temperature thermodynamic properties of CeF_3 and have reported S^{o}_{298} for CeF_3 to be 27.5 calories per mole degree. This value will be used as an estimate of S^{o}_{298} for the fluorides under consideration in this work. The tabulations of the thermodynamic functions at fifty degree intervals are given for the fluorides in Tables 4-10.

Heat of sublimation

If the free energy functions of both the solid and gaseous phases of a material are known, the standard heat of sublimation of this material may be calculated from vapor pressure measurements provided that the material does not dissociate or disproportionate in the gaseous state. This calculation is generally known as the Third Law heat of sublimation. The sublimation reaction for a rare earth fluoride may be written as follows:

$$RF_3(s) \longrightarrow RF_3(g) \qquad (24)$$

The standard heat of sublimation for reaction 24 may then be

calculated from the free energy functions

$$\Delta\left(\frac{F_T^o - H_{298}^o}{T}\right)_{reaction} = \left(\frac{F_T^o - H_{298}^o}{T}\right)_{RF_3(g)} - \left(\frac{F_T^o - H_{298}^o}{T}\right)_{RF_3(s)} \quad (25)$$

Rearranging

$$\Delta\left(\frac{F_T^o - H_{298}^o}{T}\right)_{reaction} = \left(\frac{\Delta F_T^o}{T}\right)_{reaction} - \left(\frac{\Delta H_{298}^o}{T}\right)_{reaction} \quad (26)$$

But

$$\left(\frac{\Delta F_T^o}{T}\right)_{reaction} = -R\ln K = -R\ln\left(f_{RF_3(g)}\right) \quad (27)$$

Since the vapor pressure is small, the gas pressures are low enough so that the gas may be treated as an ideal gas. Therefore, equation 27 becomes

$$\left(\frac{\Delta F_T^o}{T}\right)_{reaction} = -R\ln\left(P_{RF_3(g)}\right) \quad (28)$$

where $P_{RF_3(g)}$ is the vapor pressure of the rare earth fluoride in atmospheres. The standard heat of sublimation may now be calculated by combining equations 26 and 28.

$$\Delta H_{298}^o = -\left\{RT\ln P_{RF_3(g)} + \Delta\left[\frac{F_T^o - H_{298}^o}{T}\right]_{reaction}\right\} \quad (29)$$

The free energy functions of some of the solid rare earth fluorides have been calculated from the heat content data of this work and are given in Tables 4-10. The free energy functions for gaseous LaF_3 and CeF_3 have been calculated by Mar and Searcy (50) and Lim and Searcy (51) from spectroscopy data. Unfortunately, spectroscopy data is not currently

available for the other rare earth fluorides. Since the properties of the gaseous rare earth trifluorides should be similar, it was assumed that the free energy functions for the other rare earth fluorides should be approximately the same as those for LaF_3 and CeF_3.

In order to be able to calculate the free energy change for the sublimation reaction, the rare earth trifluoride must be the main vapor species and disproportionation or dissociation reactions must not take place. Of the seven fluorides used in the heat content work, Margrave et al. (44-49) have determined the vapor pressure of YF_3, LaF_3, NdF_3, HoF_3 and LuF_3 by both mass spectrographic and microbalance measurements. Skinner (53) has determined the vapor pressure of PrF_3. Both Skinner and Margrave reported the principle vapor species to be the trifluoride. No vapor pressure data is currently available in the literature for GdF_3.

The standard heats of sublimation were determined for YF_3, LaF_3, PrF_3, NdF_3, HoF_3 and LuF_3 using the Third Law (free energy function) method. The results of these calculations are given in Table 11. The literature values from work of Margrave (44-49) and Skinner (53) are given for comparison. The errors in the standard heat of sublimation from this work are based on a possible uncertainty of 15% in the estimated gaseous free energy functions. The errors in the literature values are those given by the authors.

Table 11. Standard heats of sublimation of some rare earth trifluorides

Salt	$H^{o}_{sub,298^{o}K.}$ (Literature value)	$H^{o}_{sub,298^{o}K.}$ (This work)
YF_3	115 ± 5 Kcal per mole	102 ± 5 Kcal per mole
LaF_3	107.5 ± 4	102 ± 5
PrF_3	107 ± 5	103 ± 5
NdF_3	95.6 ± 4	98 ± 5
HoF_3	113 ± 3	104 ± 5
LuF_3	104 ± 3	101 ± 5

DISCUSSION

Because of the large discrepancies in the values reported for the melting points and transition temperatures of the rare earth trifluorides over the years, the transition temperatures and melting points were determined by differential thermal analysis using the higher purity materials obtained in this work. The results of these determinations were given in Table 2 and Figure 6. The values for the melting points were in good agreement with the previous work of Dennison, but the values for the transition temperatures were slightly higher than those found by Thoma and Brunton (33) using high temperature x-ray diffraction.

No orthorhombic-hexagonal transition was found by DTA in LaF_3, CeF_3, PrF_3, NdF_3, EuF_3, TbF_3, DyF_3 and HoF_3. Although no transition has ever been reported for LaF_3, CeF_3, PrF_3 and NdF_3, the orthorhombic-hexagonal transition has been detected for EuF_3, TbF_3, DyF_3 and HoF_3 using high temperature x-ray techniques. The fact that the transition was not seen in the DTA data does not necessarily indicate that there is no latent heat of transition. In order to be seen with the DTA apparatus, the heat of transition must be on the order of 300-500 calories per mole, or greater.

The room temperature lattice parameters of the rare earth fluorides were determined and the results were given in Table 3. In general, the parameters obtained in this work are

in good agreement with the values obtained in other investigations (38,41,42,43). In view of this agreement, it would appear that a decrease in oxygen content in the fluorides has little or no effect on the lattice parameters. Although the exact oxygen content of the fluorides used in the other investigations was not known, analysis of fluorides prepared in the same manner as described in the papers showed the probable oxygen content to be on the order of 100-500 ppm by weight. Analyses of the fluorides prepared in this work showed only 10-50 ppm oxygen by weight. No comparison of other impurity levels could be made.

From the comparison of the enthalpies of α-Al_2O_3 measured in this work to other values, it appeared that the calorimeter was functioning properly and was a suitable instrument for the measurement of high temperature heat contents. The largest source of error in the heat content measurements was introduced from the temperature measurement of the sample. A five degree error in the sample temperature could result in an error of approximately 100 calories per mole in the heat content.

The heats of transition and fusion were obtained by computing the enthalpies at the transition temperatures using the empirical equations which defined the heat contents above and below the transition temperature. The errors in the heats of transition were computed from the uncertainties in the heat contents on either side of the transition and were found

to be approximately ± 100 calories per mole.

The heat contents of PrF_3, NdF_3 and GdF_3 have previously been measured over a temperature range of 500-1200°K. by Chaudhuri (55). The results obtained in this work for the heat contents of PrF_3 and NdF_3 are in good agreement, in the range where they can be compared, with those of Chaudhuri. However, the values obtained in this work for GdF_3 are approximately 10% lower than those obtained by Chaudhuri. The explanation for this difference is not apparent, especially in view of the good agreement for PrF_3 and NdF_3.

A plot of the entropies of transition for the orthorhombic-hexagonal transition is presented in Figure 15. With the limited number of data points available, it is difficult to make any correlations. However, if the fact that the orthorhombic-hexagonal transition in Tb and Dy was not seen by DTA is taken into account, it would appear that the entropy of transition goes through a minimum in the neighborhood of DyF_3 or HoF_3. It should be noted that the entropy of transition of YF_3 is greater than the entropy of fusion. It is also interesting that the YF_3 crystals shatter violently on cooling through the transition indicating a large change in volume. If data for the change in volume for the transition were available, it might be possible to explain the differences in magnitude of entropies of transition. The entropies of fusion and the sum of the entropies of fusion and transition are also

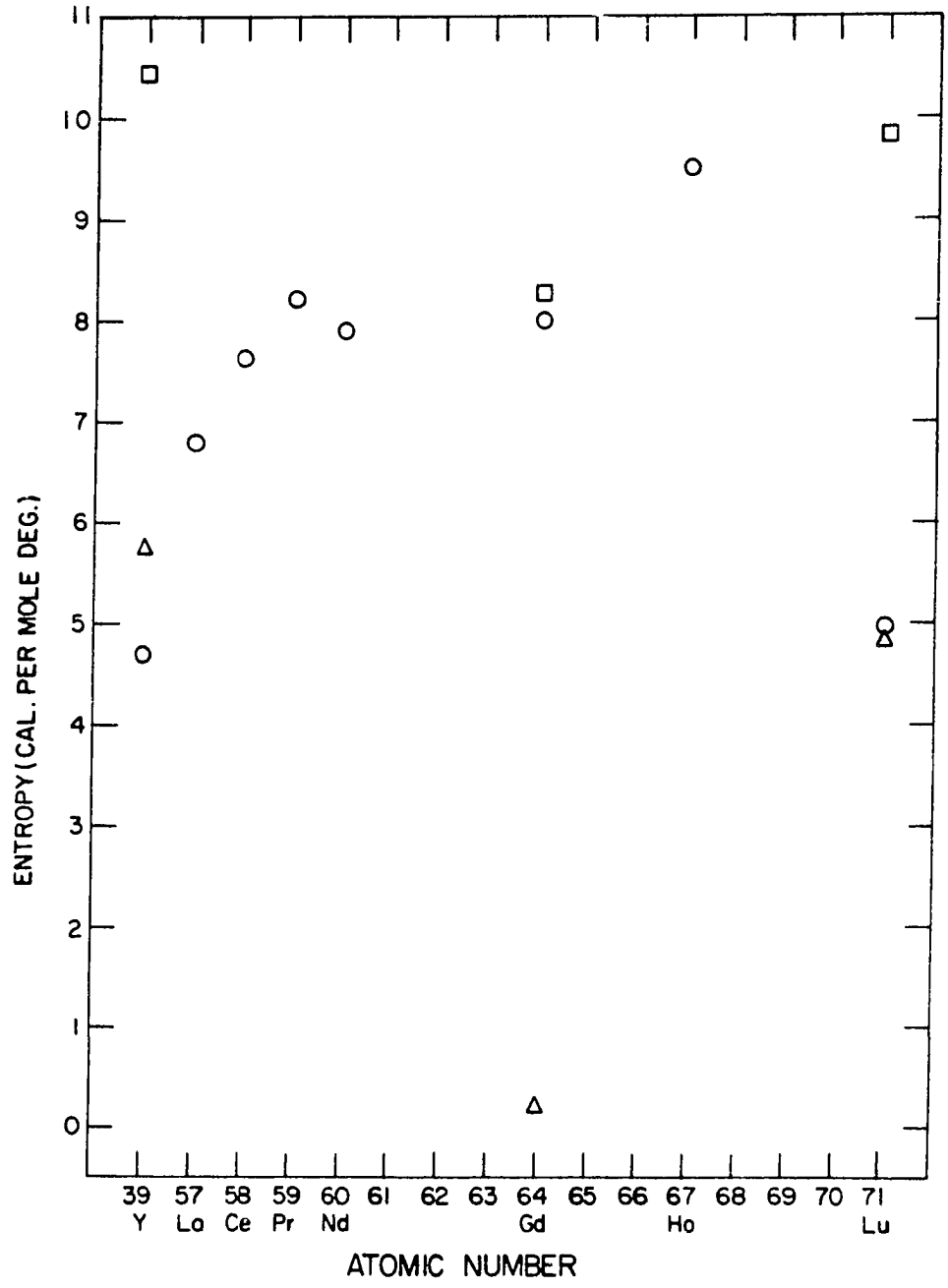

Figure 15. A comparison of the entropies of transition and fusion for the rare earth trifluorides

$\Delta = \Delta S^{o}_{Tr}$; o = ΔS^{o}_{fus}; ◘ = $\Delta S^{o}_{Tr} + \Delta S^{o}_{fus}$

plotted in Figure 15.

Although one might expect the entropies of fusion to be similar for the rare earth fluorides since they transform from a hexagonal (trigonal) phase to the liquid upon melting, this does not seem to be the case. From the limited thermodynamic data available at this time, it would appear that the entropies of fusion might be divided into two groups. The entropy of fusion appears to increase with respect to atomic number going from LaF_3 to PrF_3 but then decreases for NdF_3. Including some very qualitative DTA data, one might further speculate that the entropy of fusion increases from SmF_3 to HoF_3 but then decreases from HoF_3 to LuF_3. The reason for these maximums is not apparent. In order to explain this behavior, thermodynamic data for all of the rare earth fluorides must be available. In addition, data for the change in volume at the melting point and information on the crystal structure of the solid just below the melting point might help explain the observed entropies.

SUMMARY

In an attempt to characterize the rare earth trifluorides, a number of the physical and thermodynamic properties have been determined. The transition temperatures and the melting points of the trifluorides were determined by means of differential thermal analysis. The results were in reasonable agreement with those obtained in other work.

The lattice parameters of the rare earth trifluorides were determined by the powder method using x-ray diffraction. The light rare earth trifluorides, LaF_3 through NdF_3, were found to possess trigonal symmetry while YF_3 and the heavy trifluorides, SmF_3 through LuF_3, were found to be orthorhombic. The results were in reasonable agreement with previous work indicating that a reduction in the oxygen content has little or no effect on the lattice parameters.

This study has also described the design, method of use, and the calibration of an adiabatic copper block drop calorimeter. The calorimeter was calibrated with α-Al_2O_3 and the results were in agreement with the National Bureau of Standards data within experimental error.

The thermodynamic properties of YF_3, LaF_3, PrF_3, NdF_3, GdF_3, HoF_3 and LuF_3 were determined from a study of their heat contents as a function of temperature over a range of 100-1600^{o}C. The heats of transition and of fusion were calculated from the enthalpy curves used to describe the data.

The thermodynamic studies did not reveal an orthorhombic-hexagonal transition for LaF_3, PrF_3 or NdF_3. However, a discontinuity in the heat content curve was found for GdF_3, YF_3 and LuF_3 which was believed to correspond to the orthorhombic-hexagonal transition. Although there was no discontinuity in the heat content curve for HoF_3, there was an apparent change in slope at a temperature corresponding to the transition temperature. The latent heat of transition for YF_3 differs from the rest of the fluorides in that its magnitude is greater than that for the heat of fusion.

An attempt has been made to correlate the high temperature properties of the rare earth fluorides. However, thermodynamic data for the rest of the rare earth fluorides must be available before more meaningful correlations may be made.

LITERATURE CITED

1. Moissan, H. and A. Etard, Compt. rend. 122, 153 (1896).

2. Moissan, H., Compt. rend. 123, 184 (1986).

3. Moissan, H., Compt. rend. 131, 597 (1900).

4. Von Wartenburg, H., Naturwissenshaften 29, 271 (1941).

5. Zalkin, A. and D. H. Templeton, J. Amer. Chem. Soc. 75, 2453 (1953).

6. Spedding, F. H. and A. H. Daane, Prog. Nucl. Ener. 1, 413 (1956).

7. Carlson, O. N. and F. A. Schmidt, in "The Rare Earths," F. H. Spedding and A. H. Daane, Eds., John Wiley and Sons, New York, N.Y., 1961, Chapter 6.

8. Smutz, M., G. Burnet, J. Walker, R. Tischer, and E. Olson, Preparation of Low Content Yttrium Fluoride, U.S. Atomic Energy Commission Report ISC-1068, Iowa State University, Ames, Iowa, 1958.

9. Walker, J. and E. Olson, Preparation of Yttrium Fluoride Using Ammonium Bifluoride, U.S. Atomic Energy Commission Report IS-2, Iowa State University, Ames, Iowa, 1959.

10. Thoma, R. E., G. M. Herbert, H. Insley and C. F. Weaver, Inorg. Chem. 2, 1005 (1963).

11. Thoma, R. E. and G. M. Herbert, Inorg. Chem. 5, 1222 (1966).

12. Thoma, R. E. and R. H. Karraker, Inorg. Chem. 5, 1933 (1966).

13. Thoma, R. E. and G. D. Brunton, Inorg. Chem. 5, 1937 (1966).

14. Cunningham, B. B., D. C. Feay and M. A. Rollier, J. Amer. Chem. Soc. 76, 3361 (1954).

15. Perras, T. and C. Naeser, J. Amer. Chem. Soc. 74, 3964 (1952).

16. Popovici, J., Chem. Ber. 41, 634 (1908).

17. Daane, A. H. and F. H. Spedding, J. Electrochem. Soc. 100, 442 (1953).

18. Staritzky, E. and L. B. Asprey, Anal. Chem. 29, 855 (1957).

19. Weigel, F. and V. Scherrer, Radiochim. Acta 7, 40 (1967).

20. Popov, A. I. and G. Glockler, J. Amer. Chem. Soc. 74, 1357 (1952).

21. Tischer, R. L. and G. Burnet, Preparation of Yttrium Fluoride Using Fluorine, U.S. Atomic Energy Commission Report IS-8, Iowa State University, Ames, Iowa, 1959.

22. Asprey, L. B. and B. B. Cunningham, in "Progress in Inorganic Chemistry," Vol. II., F. Albert Cotton, Ed., Interscience, New York, N.Y., 1960.

23. Popov, A. I. and G. E. Knudson, J. Amer. Chem. Soc. 76, 3921 (1954).

24. Moriarty, J. L., J. of Met. 20(11), 41 (1968).

25. Guggenheim, H., J. Appl. Phys. 34, 2842 (1963).

26. Warshaw, S. I. and R. E. Jackson, Rev. Sci. Instr. 36, 1774 (1965).

27. Robinson, M. and D. M. Cripe, J. Appl. Phys. 37, 2072 (1966).

28. Muir, H. M. and W. Stein, Optical and Physical Properties of Single Crystal Lanthanum Trifluoride, in Proceedings of the Fifth Rare Earth Conference, Book 1, Ames, Iowa, August 30 - September 1, 1965, pp. 123 - 136.

29. Carlson, O. N., F. A. Schmidt and F. H. Spedding, Preparation of Yttrium Metal by Reduction of Yttrium Trifluoride with Calcium, U.S. Atomic Energy Commission Report ISC-744, Iowa State University, Ames, Iowa, 1956.

30. Love, B., Sci. 129, 842 (1959).

31. Powell, J. E. and F. H. Spedding, Chem. Eng. Prog. 55(24), 101 (1959).

32. Dahlmann, W. E. and V. A. Fassel, Determination of Oxygen in Rare Earth Trifluorides, Institute for Atomic Research and Department of Chemistry, Iowa State University, Ames, Iowa, manuscript in preparation.

33. Thoma, R. E. and G. D. Brunton, Inorg. Chem. 5, 1937 (1966).

34. Oftedal, I., Z. physik. Chem. B5, 272 (1929)

35. Oftedal, I., Z. physik. Chem. B13, 190 (1931).

36. Schlyter, K., Arkiv. Kemi 5, 73 (1953).

37. Templeton, D. H. and C. H. Dauben, J. Amer. Chem. Soc. 75, 4560 (1953).

38. Zalkin, A. and D. H. Templeton, Inorg. Chem. 5, 1467 (1966).

39. Mansmann, M., Z. Anorg. Allg. Chem. 331, 98 (1964).

40. Mansmann, M., Z. Krist. 122, 375 (1965).

41. Zalkin, A. and D. H. Templeton, J. Amer. Chem. Soc. 75, 2453 (1953).

42. Staritzky, E. and L. B. Asprey, Anal. Chem. 29, 856 (1957).

43. Staritzky, E. and L. B. Asprey, Anal. Chem. 29, 855 (1957).

44. Kent, R. A., K. Zmbov, J. D. McDonald, G. Besenbruch, T. C. Ehlert, R. G. Bautista, A. S. Kana'an and J. L. Margrave, in "Nuclear Applications of Nonfissionable Ceramics," A. Boltov and J. H. Handwerk, Eds., American Nuclear Society, Hinsdale, Ill., 1966, pp. 249 - 255.

45. Kent, R. A., K. Zmbov, J. D. McDonald, G. Besenbruch, A. S. Kana'an and T. L. Margrave, J. Inorg. Nucl. Chem. 28, 1419 (1966).

46. Zmbov, K. F. and J. L. Margrave, J. Chem. Phys. 45, 3167 (1966).

47. Zmbov, K. F. and J. L. Margrave, J. Phys. Chem. 70, 3379 (1966).

48. Besenbruch, G., T. V. Charlev, K. F. Zmbov and J. L. Margrave, J. Less-Com. Met. 12, 375 (1967).

49. Zmbov, K. F. and J. L. Margrave, J. Less-Com. Met. 12, 494 (1967).

50. Mar, R. W. and A. W. Searcy, J. Phys. Chem. 71, 888 (1967).

51. Lim, M. and A. W. Searcy, J. Phys. Chem. 70, 1762 (1966).

52. Suvorov, A. V., E. V. Krzhizhanovskaya and G. I. Novikov, Rus. J. Inorg. Chem. 11, 1441 (1966).

53. Skinner, H. B., Heat of Sublimation and the Evaporation Coefficient of Praseodymium Trifluoride, U.S. Atomic Energy Commission Report UCRL-17804, University of California at Berkeley, Berkeley, California, September, 1967.

54. Rudzitis, E. and E. H. Van Deventer, Materials Chemistry and Thermodynamics, U.S. Atomic Energy Commission Report ANL-7425, pp. 122 - 123, Argonne National Laboratory, Chicago, Illinois, 1967.

55. Chaudhuri, A. K., High Temperature Thermodynamic Properties of Rare Earth Fluorides, Unpublished Ph.D. thesis, Library, Iowa State University of Science and Technology, Ames, Iowa, 1967.

56. King, E. G. and A. L. Christensen, High Temperature Heat Capacity of Cerium Trifluoride, Bureau of Mines Bulletin 5510, 1959.

57. Westrum, E. F. and A. F. Beale, Jr., J. Phys. Chem. 65, 353 (1961).

58. Cavallaro, U., Atti. accad. Italia Rend. 4, 520 (1943).

59. Butler, C. P. and E. C. Y. Inn, Radiometric Method for Determining Specific Heat at Elevated Temperatures, U.S. Atomic Energy Commission Report USNRDL-TR-235, National Radiological Defence Laboratory, San Francisco, California, 1958.

60. West, E. D. and D. C. Ginnings, J. Res. Natl. Bur. Stds. 60, 309 (1958).

61. Stansbury, E. E., D. L. McElroy, M. L. Ricklesimer, G. E. Elder and R. E. Parvel, Rev. Sci. Instr. 30, 121 (1959).

62. Backhurst, I., J. Iron Steel Inst. 189, 124 (1958).

63. Braun, M., R. Kohlhass and O. Vollvex, Z. Angew. Phys. 25, 365 (1968).

64. Worthing, A. G. Phys. Rev. 12, 199 (1928).

65. Avramescu, A., Z. Tech. Physik 20, 213 (1939).

66. Wallace, A. C., P. H. Sidley and G. C. Davidson, J. Appl. Phys. 31, 168 (1960).

67. Spedding, F. H., J. J. McKeown and A. H. Daane, J. Phys. Chem. 64, 289 (1960).

68. White, W. P., The Modern Calorimeter, Chemical Catalog Company, New York, 1928.

69. Jaeger, F. M. and E. Rosenbohm, On the Exact Determination of the Specific Heats of Solid Substances between 0° and 1625°C. in Method and Apparatus, Proc. Acad. Sci., Amsterdam, 30, 305 (1927).

70. Southard, J. C., J. Amer. Chem. Soc. 19, 268 (1922).

71. Kelley, K. K., B. F. Naylor and C. H. Shomate, The Thermodynamic Properties of Manganese, Bureau of Mines Tech. Paper 686, 1946.

72. Maier, C. G. and K. K. Kelley, J. Amer. Chem. Soc. 54, 3243 (1932).

73. Furukawa, G. T., T. B. Douglas, R. E. McClaskey and D. C. Ginnings, J. Res. Natl. Bur. Stds. 57, 67 (1956).

74. Yvon, K., W. Jeitschko and E. Parthe, A Fortran IV Program for the Intensity Calculation of Powder Patterns (1969 Version), University of Pennsylvania, Laboratory for Research on the Structure of Matter, ca. 1969.

75. Vogel, R. E. and C. P. Kempter, Acta Cryst. 14, 1130 (1931).

ACKNOWLEDGMENT

The author wishes to thank Dr. F. H. Spedding for his advice and criticism during the course of this work and Dr. K. A. Gschneidner for his advice and for the loan of some of his equipment. The author also wishes to thank Jack Moorman for his assistance with the differential thermal analysis data, Dale McMasters for his assistance with the x-ray work, Les Reid, George Ahrens and Paul Palmer for their help in fabricating the platinum parts and the members of the various analytical groups for analyzing the fluorides. Special thanks are extended to B. Beaudry for acting as a sounding board for ideas and offering many constructive suggestions. The author also wishes to thank his wife for typing this thesis and for her encouragement and understanding.

APPENDIX A

ANALYSES OF SOME RARE EARTH FLUORIDES

Methods of Analysis

Wet Chemical Analysis[1]

Chemical analyses of the rare earth fluorides by wet methods were carried out by W. C. Diedricks, K. Hopkins and G. Austin under the supervision of Mr. R. Bachman and Dr. C. V. Banks. Due to the insolubility and high stability of the rare earth fluorides, the precision was ± 5%.

Helium Fusion Analysis[2]

Oxygen analyses of the rare earth fluorides were carried out by C. Hill under the supervision of W. E. Dahlmann and Dr. V. A. Fassel. At the time the samples were run, the helium fusion technique for fluorides was in the development stage. As a result the lower limit for accurate results was on the order of 20 ppm and although the order of magnitude of the oxygen analyses should have been correct, the actual value might be off by as much as a factor of two, especially at the lower concentrations.

---

[1]Banks, C. V., private communication, Ames Laboratory, Iowa State University, Ames, Iowa, 1969.

[2]Dahlmann and Fassel (32).

Mass Spectrographic Analysis[1]

The mass spectrographic analyses of the rare earth fluorides were carried out by R. Conzemius and J. Cappellen under the supervision of Dr. H. J. Svec. This method was used to analyze for all impurities except carbon and oxygen.

Table 12 lists the impurities in the rare earth fluorides used in the thermodymanic studies. Elements not listed were either not detected or present in quantities less than 1 ppm by weight.

Table 12. Analyses of some rare earth fluorides in ppm by weight

Impurity	YF_3	LaF_3	PrF_3	NdF_3	GdF_3	HoF_3	LuF_3
C	1	N.D.	N.D.	N.D.	<5	<5	<5
O	17	22	47	52	33	6	5
Na	5	10	5	20	50	36	54
Al	1	.5	2	9	30	12	6
Cl	2	N.D.	10	7	10	10	12
K	2	N.D.	3	5	1	2	3
Ca	25	9	10	28	14	30	30
Sc	.5	.1	2	2	2	6	5
Ti	.1	N.D.	.7	3	<4	.9	2
Cr	6	N.D.	7	<10	2	2	.8
Mn	.5	N.D.	2	3	1	N.D.	.2
Fe	4	1	4	4	18	10	2
Co	N.D.	N.D.	2	N.D.	2	N.D.	.2
Ni	6	N.D.	.1	.4	.1	.3	.3
Cu	.6	N.D.	.5	.9	2	.7	.4
Zn	.5	N.D.	.2	1	.2	.2	.3
Y		3	4	4	2	5	9
Mo	N.D.	6	N.D.	N.D.	N.D.	N.D.	N.D.

[1]Svec, H. J., private communication, Ames,Laboratory, Iowa State University, Ames, Iowa, 1969.

Table 12 (continued).

Impurity	YF_3	LaF_3	PrF_3	NdF_3	GdF_3	HoF_3	LuF_3
La	3	--	3	20	N.D.	.7	.5
Ce	2	8	2	3	N.D.	.2	.5
Pr	2	30	--	20	20	7	6
Nd	5	5	70	--	1	30	40
Sm	N.D.	N.D.	N.D.	5	2	3	5
Eu	N.D.	.8	N.D.	<1	10	.2	N.D.
Gd	N.D.	N.D.	6	<10	--	4	3
Tb	2	1	.8	<1	20	.5	.4
Dy	9	N.D.	2	<10	2	6	2
Ho	<20	N.D.	<6	<20	2	--	3
Er	4	5	2	<6	9	N.D.	1
Tm	N.D.	N.D.	1	<10	17	N.D.	.2
Yb	N.D.	N.D.	N.D.	<1	<20	N.D.	N.D.
Lu	N.D.	N.D.	N.D.	<1	<20	20	--
Ta	N.D.	N.D.	.9	N.D.	.2	.4	.4
W	N.D.	N.D.	N.D.	N.D.	2	N.D.	N.D.
Pt	N.D.	30	N.D.	N.D.	N.D.	N.D.	N.D.
Total R.E.	60.6	71.0	71.2	71.6	73.1	78.8	74.7
Total F^-	39.2	29.1	28.8	28.3	26.8	25.4	25.2

APPENDIX B

SUMMARY OF THE POWDER DATA

The data from the powder patterns used to calculate the lattice parameters of the rare earth trifluorides is given in Tables 13-25. The powder patterns were indexed on the basis of either a trigonal cell which was isostructural with LaF_3 or a orthorhombic cell which was isostructural with YF_3. The unit cells of LaF_3 and YF_3 were determined from single crystal work by other experimenters.

In the backreflection region of the actual powder patterns each $\sin^2\theta$ value corresponding to a given hkl was resolved into two components due to the Kα1 wavelength and the Kα2 wavelength. To simplify the tables, the $\sin^2\theta$ values due to the Kα1 and Kα2 wavelengths were converted to $\sin^2\theta$ values based on the Kα mean wavelength. The initial value at which this was done is noted in each table.

Table 13. Yttrium fluoride orthorhombic powder pattern

hkl	$\sin^2\theta^a$ obs	$\sin^2\theta^a$ calc	I^o_{obs}	hkl	$\sin^2\theta^a$ obs	$\sin^2\theta^a$ calc	I^o_{obs}
011	0.0443	0.0434	M	341	0.3667	0.3648	M
101	0.0463	0.0454	S	250	0.3760	0.3744	W
020	0.0514	0.0505	S	223	0.3874	0.3861	M
111	0.0592	0.0581	VS	422	0.4105	0.4082	M
210	0.0726	0.0713	S	440	0.4378	0.4367	W
121	0.0971	0.0960	M	521	0.4486	0.4478	W
211	0.1034	0.1020	W	152	0.4551	0.4536	M
220	0.1104	0.1092	W	060		0.4538	
002	0.1248	0.1231	M	252	0.4982	0.4975	W
221	0.1414	0.1400	S	161	0.5009	0.5002	W
112	0.1519	0.1504	S	531	0.5113	0.5110	W
131	0.1608	0.1591	VS	260	0.5140	0.5134	W
301	0.1643	0.1627	S	114	0.5205	0.5197	W
230	0.1738	0.1723	VS	413	0.5244	0.5242	M
022		0.1736		600	0.5270	0.5278	VW
311	0.1771	0.1754	VS	243	0.5384	0.5377	W
122	0.1900	0.1883	S	522	0.5401	0.5402	M
212	0.1958	0.1944	S	610		0.5404	
040	0.2038	0.2021	S	024	0.5431	0.5429	M
321	0.2148	0.2133	S	442	0.5605	0.5598	W
400	0.2360	0.2346	M	352	0.5704	0.5708	VW
141	0.2491	0.2476	W	611	0.5736	0.5712	VW
132	0.2529	0.2514	W	062	0.5787	0.5778	VW
302	0.2563	0.2550	VW	451	0.5813	0.5812	VW
312	0.2690	0.2677	M	053	0.5929	0.5928	W
331	0.2783	0.2764	M	541	0.5985	0.5994	VW
411		0.2780		532	0.6032	0.6033	VW
420	0.2862	0.2851	W	153	0.6083	0.6074	VW
241	0.2918	0.2915	W	343	0.6108	0.6110	VW
232	0.2970	0.2954	M	361	0.6176	0.6175	M
322	0.3066	0.3056	W	134[b]	0.6206	0.6207	M
042	0.3272	0.3252	W	433[b]	0.6258	0.6252	M
203	0.3375	0.3356	W	314	0.6382	0.6370	VW
402	0.3583	0.3577	W	630	0.6419	0.6415	MW
151	0.3621	0.3612	W	171	0.6648	0.6644	M

[a]Copper Kα mean radiation (λ = 1.54178 Å); a = 6.367; b = 6.859; c = 4.394.

[b]From this value on, the observed $\sin^2\theta$ values were resolved into the Kα1 and Kα2 components.

Table 13 (continued)

hkl	$\sin^2\theta$ obs	$\sin^2\theta$ calc	I^o_{obs}	hkl	$\sin^2\theta$ obs	$\sin^2\theta$ calc	I^o_{obs}
270	0.6785	0.6786	MW	650	0.8441	0.8436	M
460	0.6895	0.6893	W	225	0.8784	0.8785	M
144	0.7106	0.7092	M	073	0.8965	0.8959	W
362		0.7098		281	0.8980	0.8979	W
334	0.7389	0.7380	W	524	0.9047	0.9094	S
701	0.7499	0.7492	W	082	0.9320	0.9316	W
632	0.7653	0.7646	WM	182	0.9465	0.9462	W
371	0.7825	0.7817	M	741	0.9512	0.9513	M
015		0.7820		553	0.9596	0.9593	W
263	0.7911	0.7904	W	652	0.9669	0.9667	S
721	0.8000	0.7997	M	381	0.9714	0.9712	S
462	0.8124	0.8124	VW	534		0.9726	
154	0.8233	0.8228	M	820	0.9888	0.9889	M
453	0.8274	0.8274	S				
205		0.8279					

Table 14. Lanthanum fluoride trigonal powder pattern

hkl	$\sin^2\theta$[a] obs	calc	I^o_{obs}	hkl	$\sin^2\theta$[a] obs	calc	I^o_{obs}
002	0.0442	0.0440	M	226	0.5794	0.5801	VVW
110	0.0464	0.0460	M	117	0.5846	0.5849	VW
111	0.0574	0.0570	VS	334	0.5902	0.5904	VW
112	0.0906	0.0900	W	602[b]		0.5962	
121	0.1186	0.1184	VVW	145	0.5976	0.5969	WB
300	0.1385	0.1381	S	250		0.5983	
113	0.1455	0.1450	VS	521	0.6091	0.6092	WVW
004	0.1766	0.1760	VW	252	0.6430	0.6424	VVW
302	0.1820	0.1821	S	253	0.6966	0.6971	WM
221	0.1956	0.1952	MS	416	0.7188	0.7177	VVW
114	0.2226	0.2220	VW	227	0.7230	0.7225	VW
222	0.2285	0.2282	VVW	604	0.7281	0.7280	VW
223	0.2836	0.2832	M	441	0.7480	0.7473	VW
304	0.3148	0.3141	M	524	0.7746	0.7738	VVW
410	0.3222	0.3223	WM	336	0.8103	0.8098	WM
411	0.3332	0.3333	M	443	0.8356	0.8352	WVW
224	0.3611	0.3601	VVW	308	0.8425	0.8414	WVW
142	0.3670	0.3663	VVW	417	0.8611	0.8606	MW
006	0.3966	0.3969	VVW	525	0.8731	0.8730	M
330	0.4151	0.4144	WM	171	0.8854	0.8854	MW
413	0.4220	0.4213	M	444	0.9127	0.9121	VVW
116	0.4423	0.4420	VW	712	0.9185	0.9183	VVW
332	0.4593	0.4584	M	119	0.9364	0.9361	M
225		0.4591		066	0.9482	0.9479	SM
414	0.4990	0.4983	VW	630	0.9666	0.9664	SM
306	0.5343	0.5340	VVW	173	0.9739	0.9733	VS
600	0.5530	0.5526	VW	526	0.9940	0.9938	M

[a]Copper Kα mean radiation (λ = 1.54178 Å); a = 7.186; c = 7.352.

[b]From this value on, the observed $\sin^2\theta$ values were resolved into the Kα1 and Kα2 components.

Table 15. Praseodymium fluoride trigonal powder pattern

hkl	$\sin^2\theta$[a] obs	calc	I^o_{obs}	hkl	$\sin^2\theta$[a] obs	calc	I^o_{obs}
002	0.0455	0.0545	MS	306	0.5511	0.5506	W
110	0.0480	0.0474	MS	600[b]	0.5691	0.5694	VW
111	0.0593	0.0588	VS	111[b]	0.6034	0.6031	VVW
112	0.0932	0.0928	W	334	0.6088	0.6085	VVW
202	0.1091	0.1086	VVW	415	0.6160	0.6147	WM
121	0.1222	0.1220	VW	521	0.6283	0.6282	WVW
300	0.1431	0.1424	S	252	0.6626	0.6622	VVW
113	0.1500	0.1495	S	253	0.7188	0.7189	WVW
004	0.1824	0.1814	VW	146	0.7402	0.7404	VW
032	0.1886	0.1877	SM	227	0.7453	0.7455	VW
221	0.2022	0.2011	MS	604	0.7504	0.7508	VW
114	0.2296	0.2289	VVW	441	0.7701	0.7705	VVW
222	0.2361	0.2352	VVW	118	0.7735	0.7732	VVW
223	0.2926	0.2919	M	524	0.7979	0.7983	VVW
304	0.3244	0.3238	MW	336	0.8354	0.8353	W
115	0.3319	0.3310	MW	443	0.8617	0.8617	WVW
411	0.3442	0.3435	M	308	0.8683	0.8681	WVW
224	0.3711	0.3712	VVVW	417	0.8876	0.8878	WM
142	0.3777	0.3775	VVW	255	0.9002	0.9003	WM
006	0.4090	0.4082	VW	711	0.9130	0.9129	WM
330	0.4267	0.4270	VWW	444	0.9406	0.9406	VVVW
413	0.4346	0.4342	WM	712	0.9466	0.9469	VW
116	0.4557	0.4557	VWW	119	0.9660	0.9660	MW
332	0.4736	0.4724	WM	606	0.9776	0.9776	WM
144	0.5134	0.5136	VVW				

[a]Copper Kα mean radiation (λ = 1.54178 Å); a = 7.078; c = 7.239.

[b]From this value on, the observed $\sin^2\theta$ values were resolved into their Kα1 and Kα2 components.

Table 16. Neodymium fluoride trigonal powder pattern

hkl	$\sin^2\theta$[a] obs	calc	I^o_{obs}	hkl	$\sin^2\theta$[a] obs	calc	I^o_{obs}
002	0.0464	0.0458	MS	117	0.6099	0.6096	VW
110	0.0486	0.0481	WVW	334	0.6163	0.6169	VVW
111	0.0601	0.0596	S	602	0.6234	0.6630	WM
112	0.0946	0.0940	VW	415		0.6233	
300	0.1454	0.1443	MS	521	0.6369	0.6367	W
113	0.1522	0.1513	VS	253	0.7278	0.7283	W
004	0.1845	0.1834	W	146	0.7492	0.7495	VW
032	0.1910	0.1902	M	227	0.7537	0.7543	WVW
221	0.2045	0.2039	W	604	0.7615	0.7617	VW
114	0.2326	0.2315	VW	441	0.7815	0.7812	W
222	0.2389	0.2382	VVW	524	0.8090	0.8088	VVW
223	0.2968	0.2956	M	336	0.8457	0.8457	MW
304	0.3284	0.3277	M	443	0.8722	0.8727	WVW
115	0.3362	0.3347	M	038	0.8780	0.8781	M
411	0.3490	0.3482	M	147	0.8982	0.8985	M
224	0.3763	0.3758	VVW	255	0.9107	0.9119	M
142	0.3831	0.3826	VVW	711	0.9254	0.9253	M
006	0.4134	0.4127	VVW	444	0.9531	0.9529	VVW
330	0.4336	0.4329	VW	712	0.9595	0.9598	VW
143	0.4401	0.4399	MW	534	0.9689	0.9691	VVW
116	0.4614	0.4787	WVW	119	0.9768	0.9769	S
332	0.4793	0.4790	MW	066	0.9898	0.9899	M
225		0.5201					
144[b]	0.5198	0.5201	VVW				
036	0.5574	0.5568	WM				
600	0.5782	0.5768	VVW				
226	0.6056	0.6048	VVW				

[a]Copper Kα mean radiation (λ = 1.54178 Å); a = 7.030; c = 7.200.

[b]From this value on, the observed $\sin^2\theta$ values were resolved into their Kα1 and Kα2 components.

Table 17. Samarium fluoride orthorhombic powder pattern

hkl	$\sin^2\theta$[a] obs	calc	I^o_{obs}	hkl	$\sin^2\theta$[a] obs	calc	I^o_{obs}
011	0.0953	0.0939	W	241	0.6074	0.6066	W
101	0.0978	0.0974	M	232	0.6157	0.6250	MW
020	0.1066	0.1053	M	013	0.6345	0.6345	WM
111	0.1247	0.1234	VS	322[b]	0.6412	0.6406	VVW
210	0.1453	0.1441	S	042	0.6919	0.6911	MW
121	0.2040	0.2024	W	430	0.7080	0.7080	VVW
002	0.2719	0.2704	W	142	0.7214	0.7208	WM
221	0.2919	0.2907	M	051	0.7267	0.7258	MW
112	0.3278	0.3261	M	203		0.7259	
301	0.3352	0.3327	S	402	0.7417	0.7416	VW
131		0.3340		151	0.7552	0.7554	S
230	0.3560	0.3548	M	431	0.7759	0.7759	M
311	0.3602	0.3590	W	250		0.7761	
022	0.3766	0.3757	W	501	0.8044	0.8040	VVW
122	0.4064	0.4051	WM	511	0.8314	0.8304	VS
212	0.4158	0.4145	WM	233		0.8315	
040	0.4223	0.4212	S	422	0.8468	0.8469	MW
321	0.4391	0.4380	WM	440	0.8926	0.8925	M
400	0.4722	0.4712	VW	521	0.9091	0.9092	WM
141	0.5197	0.5183	M	060	0.9479	0.9477	S
132	0.5371	0.5371	W	152	0.9581	0.9580	M
312	0.5619	0.5611	W	432	0.9787	0.9785	W
331	0.5701	0.5690	W	323		0.9787	
420	0.5774	0.5759	W	351	0.9912	0.9910	MS

[a]Chromium Kα mean radiation (λ = 2.29092 Å); a = 6.674; b = 7.059; c = 4.404.

[b]From this value on, the observed $\sin^2\theta$ values were resolved into their Kα1 and Kα2 components.

Table 18. Gadolinium fluoride orthorhombic powder pattern

hkl	$\sin^2\theta$[a] obs	calc	I^o_{obs}	hkl	$\sin^2\theta$[a] obs	calc	I^o_{obs}
011	0.0960	0.0950	W	232	0.6358	0.6357	M
101	0.0994	0.0984	M	013	0.6396	0.6394	MW
020	0.1090	0.1076	MS	322	0.6533	0.6530	W
111	0.1267	0.1253	SM	113	0.6690	0.6698	WVW
210	0.1496	0.1483	M	042	0.7026	0.7025	WM
201	0.1908	0.1895	VW	430[b]	0.7274	0.7277	VVW
121	0.2076	0.2060	MW	142[b]	0.7338	0.7329	SM
002	0.2742	0.2722	WM	051	0.7406	0.7404	VW
221	0.2987	0.2970	M	123	0.7509	0.7505	VVW
102	0.3039	0.3026	VVW	402	0.7582	0.7579	W
112	0.3311	0.3295	SM	151	0.7708	0.7707	S
301	0.3422	0.3412	VS	341		0.7715	
230	0.3648	0.3634	S	332	0.7878	0.7874	VVW
311	0.3694	0.3681	MW	250	0.7933	0.7937	WM
022	0.3812	0.3799	MW	501	0.8269	0.8269	VVW
122	0.4115	0.4102	M	223	0.8418	0.8415	S
212	0.4223	0.4206	M	511	0.8540	0.8538	MS
040	0.4318	0.4303	M	033		0.8546	
321	0.4504	0.4489	MS	422	0.8656	0.8655	M
400	0.4870	0.4856	WM	133	0.8855	0.8849	VVW
141	0.5297	0.5287	M	313	0.9122	0.9126	VVW
302	0.5462	0.5454	MW	440	0.9159	0.9159	MS
312	0.5731	0.5723	WM	521	0.9346	0.9345	MS
331	0.5830	0.5833	WM	060	0.9679	0.9681	S
420	0.5938	0.5932	WM	152	0.9743	0.9741	MS
241	0.6206	0.6197	W	323	0.9934	0.9933	WM

[a]Chromium Kα mean radiation (λ = 2.29092 Å); a = 6.575; b = 6.985; c = 4.391.

[b]From this value on, the observed $\sin^2\theta$ values were resolved into their Kα1 and Kα2 components.

Table 19. Terbium fluoride orthorhombic powder pattern

hkl	$\sin^2\theta$[a] obs	calc	I^o_{obs}	hkl	$\sin^2\theta$[a] obs	calc	I^o_{obs}
011	0.0970	0.0954	W	312	0.5794	0.5786	MW
101	0.1006	0.0992	MS	411	0.5915	0.5907	MS
020	0.1100	0.1087	S	420	0.6043	0.6041	MW
111	0.1278	0.1264	S	241[b]	0.6272	0.6270	VVW
210	0.1523	0.1510	MS	232	0.6418	0.6413	S
201	0.1938	0.1920	VVW	013		0.6410	
121	0.2092	0.2079	M	322	0.6608	0.6602	VVW
211	0.2207	0.2192	VVW	113	0.6740	0.6720	VVW
002	0.2745	0.2728	W	042	0.7080	0.7078	W
221	0.3021	0.3008	M	051	0.7473	0.7479	VW
112	0.3322	0.3310	MS	402	0.7683	0.7682	WVW
131	0.3446	0.3438	VS	151	0.7792	0.7788	WM
301	0.3479	0.3468	S	341	0.7821	0.7818	M
230	0.3697	0.3685	S	332	0.7967	0.7961	VVW
311	0.3747	0.3740	MW	250	0.8041	0.8035	WM
022	0.3828	0.3816	WM	501	0.8427	0.8422	VVW
122	0.4139	0.4125	M	223	0.8467	0.8464	S
212	0.4247	0.4238	MS	033	0.8588	0.8585	VW
040	0.4364	0.4350	MS	511	0.8703	0.8694	MS
321	0.4568	0.4556	M	422	0.8775	0.8769	MS
400	0.4960	0.4954	VW	440	0.9312	0.9314	MS
141	0.5357	0.5342	W	521	0.9514	0.9509	M
132	0.5491	0.5485	WVW	060	0.9792	0.9787	S
302	0.5513	0.5515	WVW	152	0.9827	0.9825	M

[a]Chromium Kα mean radiation (λ = 2.29092 Å); a = 6.510; b = 6.947; c = 4.386.

[b]From this value on, the observed $\sin^2\theta$ values were resolved into their Kα1 and Kα2 components.

Table 20. Dysprosium fluoride orthorhombic powder pattern

hkl	$\sin^2\theta$[a] obs	calc	I^o_{obs}	hkl	$\sin^2\theta$[a] obs	calc	I^o_{obs}
011	0.0958	0.0960	M	420[b]	0.6142	0.6130	M
101	0.0997	0.0999	S	241	0.6346	0.6345	W
020	0.1100	0.1085	S	013	0.6465	0.6441	M
111	0.1260	0.1274	S	232		0.6476	
210	0.1520	0.1533	M	322	0.6681	0.6670	VW
201	0.1948	0.1943	VW	113	0.6759	0.6755	VW
121	0.2077	0.2099	M	042	0.7146	0.7142	M
211	0.2214	0.2218	VW	142	0.7441	0.7456	M
002	0.2739	0.2740	M	203		0.7424	
221	0.3051	0.3043	M	051	0.7572	0.7563	W
112	0.3328	0.3329	MS	123		0.7580	
131	0.3480	0.3475	S	402	0.7776	0.7770	W
301	0.3520	0.3515	M	151	0.7874	0.7877	MW
230	0.3736	0.3734	SM	341	0.7919	0.7917	M
311	0.3792	0.3790	M	332	0.8051	0.8041	W
022	0.3841	0.3840	M	412		0.8047	
122	0.4151	0.4154	M	250	0.8132	0.8136	S
212	0.4275	0.4273	M	223	0.8528	0.8524	S
040	0.4406	0.4402	M	033	0.8637	0.8642	W
321	0.4616	0.4615	M	511	0.8823	0.8820	M
400	0.5037	0.5030	MW	422	0.8873	0.8872	W
141	0.5403	0.5401	M	313	0.9263	0.9271	VW
132	0.5526	0.5530	MW	440	0.9430	0.9432	M
312	0.5839	0.5845	M	521	0.9645	0.9645	M
331	0.6000	0.5991	MS				
411		0.5990					

[a]Chromium Kα mean radiation (λ = 2.29092 Å); a = 6.460; b = 6.906; c = 4.376.

[b]From this value on, the observed $\sin^2\theta$ values were resolved into their Kα1 and Kα2 components.

Table 21. Holmium fluoride orthorhombic powder pattern

hkl	$\sin^2\theta$[a] obs	$\sin^2\theta$[a] calc	I^o_{obs}	hkl	$\sin^2\theta$[a] obs	$\sin^2\theta$[a] calc	I^o_{obs}
011	0.0975	0.0962	W	302	0.5617	0.5616	VW
101	0.1016	0.1004	M	312	0.5897	0.5894	MW
020	0.1122	0.1110	S	331	0.6072	0.6062	MS
111	0.1295	0.1282	S	420	0.6225	0.6229	MW
210	0.1573	0.1557	MS	241	0.6402	0.6406	VW
201	0.1979	0.1964	VW	013	0.6431	0.6436	W
121	0.2127	0.2115	M	232	0.6511	0.6515	M
211	0.2246	0.2242	VVW	322[b]	0.6733	0.6727	W
002	0.2752	0.2737	W	042	0.7185	0.7178	WM
221	0.3085	0.3074	M	203	0.7444	0.7439	WM
112	0.3350	0.3334	M	142	0.7509	0.7498	W
131	0.3516	0.3503	VS	123	0.7595	0.7589	VVW
301	0.3579	0.3564	S	051	0.7628	0.7624	WVW
230	0.3789	0.3778	S	402	0.7859	0.7856	WM
311	0.3853	0.3841	S	151	0.7952	0.7944	MW
022		0.3847		341	0.8011	0.8005	MS
122	0.4178	0.4167	M	250	0.8229	0.8221	MW
212	0.4303	0.4294	MS	431	0.8305	0.8302	VW
040	0.4450	0.4442	MS	223	0.8556	0.8548	SM
321	0.4680	0.4674	MS	033	0.8669	0.8665	WVW
400	0.5125	0.5119	WM	422	0.8966	0.8966	SVS
141	0.5448	0.5446	M	440	0.9567	0.9561	MS
132	0.5556	0.5555	W	521	0.9792	0.9793	M

[a]Chromium Kα mean radiation (λ = 2.29092 Å); a = 6.405; b = 6.874; c = 4.378.

[b]From this value on, the observed $\sin^2\theta$ values were resolved into their Kα1 and Kα2 components.

Table 22. Erbium fluoride orthorhombic powder pattern

hkl	$\sin^2\theta$[a] obs	calc	I^o_{obs}	hkl	$\sin^2\theta$[a] obs	calc	I^o_{obs}
011	0.0980	0.0963	W	411	0.6166	0.6169	W
101	0.1024	0.1008	M	420	0.6335	0.6327	WM
020	0.1138	0.1120	S	013	0.6431	0.6427	W
111	0.1304	0.1288	S	241	0.6469	0.6466	W
210	0.1598	0.1582	MS	232	0.6560	0.6555	MW
201	0.2004	0.1984	VVW	322[b]	0.6778	0.6781	WVW
121	0.2149	0.2129	MW	042	0.7220	0.7214	WM
211	0.2283	0.2265	VVW	203	0.7449	0.7448	W
002	0.2752	0.2732	W	142	0.7543	0.7539	WVW
221	0.3126	0.3105	MW	123	0.7688	0.7593	VW
112	0.3358	0.3337	MW	430	0.7725	0.7727	VVW
131	0.3545	0.3529	VS	402	0.7939	0.7938	WVW
301	0.3624	0.3612	SM	151	0.8017	0.8011	WM
230	0.3844	0.3823	SM	341	0.8100	0.8093	M
311	0.3908	0.3892	MS	250	0.8314	0.8304	WM
122	0.4199	0.4178	M	431	0.8415	0.8410	VW
212	0.4328	0.4314	MS	223	0.8580	0.8579	S
040	0.4497	0.4482	MS	033	0.8673	0.8668	VW
321	0.4750	0.4732	MS	501	0.8822	0.8818	VW
400	0.5225	0.5206	WM	422	0.9066	0.9059	MS
141	0.5499	0.5490	MW	511	0.9103	0.9098	M
132	0.5586	0.5578	W	313	0.9364	0.9366	VW
302	0.5668	0.5660	VW	440	0.9693	0.9688	MS
312	0.5952	0.5941	M	521	0.9940	0.9938	M
331	0.6136	0.6133	MW				

[a]Chromium Kα mean radiation (λ = 2.29092 Å); a = 6.350; b = 6.844; c = 4.383.

[b]From this value on, the observed $\sin^2\theta$ values were resolved into their Kα1 and Kα2 components.

Table 23. Thulium fluoride orthorhombic powder pattern

hkl	$\sin^2\theta$[a] obs	calc	I^o_{obs}	hkl	$\sin^2\theta$[a] obs	calc	I^o_{obs}
011	0.0969	0.0957	W	331	0.6212	0.6214	M
101	0.1016	0.1007	M	411	0.6276	0.6284	WVW
020	0.1141	0.1131	S	013	0.6351	0.6353	WM
111	0.1301	0.1290	S	420	0.6460	0.6457	WM
210	0.1627	0.1614	MS	241[b]	0.6527	0.6528	VVW
201	0.2014	0.2006	VVW	232	0.6574	0.6574	MS
121	0.2148	0.2138	MS	113	0.6690	0.6686	VW
002	0.2709	0.2698	W	322	0.6823	0.6825	VW
221	0.3146	0.3137	MW	042	0.7212	0.7220	M
112	0.3321	0.3314	M	203	0.7403	0.7402	W
131	0.3561	0.3551	VS	123	0.7540	0.7534	W
301	0.3679	0.3671	S	142		0.7553	
022	0.3840	0.3829	MW	051	0.7746	0.7740	VVW
230	0.3882	0.3875	S	430	0.7872	0.7870	VVW
311	0.3959	0.3953	MS	402	0.8017	0.8025	WM
122	0.4164	0.4162	MW	151	0.8069	0.8073	M
212	0.5315	0.5312	MS	341	0.8192	0.8193	MS
040	0.4528	0.4522	M	250	0.8400	0.8398	M
321	0.4811	0.4801	M	223	0.8538	0.8533	S
400	0.5334	0.5326	W	431		0.8545	
141	0.5525	0.5530	WM	033	0.8611	0.8615	VW
132	0.5564	0.5575	VW	422	0.9146	0.9155	MS
302	0.5698	0.5694	VVW	511	0.9281	0.9280	M
312	0.5978	0.5977	M	440	0.9850	0.9849	S

[a]Chromium Kα mean radiation (λ = 2.29092 Å); a = 6.278; b = 6.813; c = 4.410.

[b]From this value on, the observed $\sin^2\theta$ values were resolved into their Kα1 and Kα2 components.

Table 24. Ytterbium fluoride orthorhombic powder pattern

hkl	$\sin^2\theta$[a] obs	$\sin^2\theta$[a] calc	I^o_{obs}	hkl	$\sin^2\theta$[a] obs	$\sin^2\theta$[a] calc	I^o_{obs}
011	0.0967	0.0952	W	331	0.6293	0.6286	M
101	0.1022	0.1007	M	013		0.6293	
020	0.1152	0.1139	S	411	0.6394	0.6384	VVW
111	0.1307	0.1292	S	420		0.6571	
210	0.1664	0.1643	MS	241	0.6586	0.6583	SM
121	0.2160	0.2146	MW	232		0.6592	
002	0.2687	0.2670	W	322[b]	0.6876	0.6865	VVW
221	0.3179	0.3165	MW	042	0.7236	0.7227	W
112	0.3310	0.3295	MW	203	0.7372	0.7366	VW
131	0.3588	0.3570	VS	123	0.7498	0.7487	VVW
301	0.3735	0.3723	S	142	0.7578	0.7567	VW
022	0.3824	0.3810	MW	051	0.7805	0.7798	VVW
230	0.3938	0.3921	S	430	0.8008	0.7998	VVW
311	0.4020	0.4008	MS	402	0.8112	0.8102	W
122	0.4165	0.4149	WM	151	0.8132	0.8128	M
212	0.4334	0.4313	MS	341	0.8289	0.8284	MS
040	0.4572	0.4557	M	250	0.8485	0.8479	W
321	0.4873	0.4862	M	223	0.8519	0.8515	M
400	0.5444	0.5432	W	033	0.8571	0.8581	VW
141	0.5574	0.5564	MW	501	0.9164	0.9165	VVW
132		0.5573		422	0.9251	0.9252	S
302	0.5730	0.5726	VVW	511	0.9446	0.9443	MS
312	0.6022	0.6011	W				

[a]Chromium Kα mean radiation (λ = 2.29092 Å); a = 6.217; b = 6.787; c = 4.433.

[b]From this value on, the observed $\sin^2\theta$ values were resolved into their Kα1 and Kα2 components.

Table 25. Lutetium fluoride orthorhombic powder pattern

hkl	$\sin^2\theta$[a] obs	calc	I^o_{obs}	hkl	$\sin^2\theta$[a] obs	calc	I^o_{obs}
011	0.0954	0.0943	W	312	0.6041	0.6038	W
101	0.1014	0.1004	M	013	0.6207	0.6191	VW
020	0.1160	0.1148	S	331	0.6375	0.6367	WM
111	0.1304	0.1291	S	411	0.6506	0.6503	VW
210	0.1689	0.1677	MS	232	0.6605	0.6598	MW
121	0.2167	0.2152	M	420	0.6717	0.6708	W
002	0.2636	0.2624	W	322[b]	0.6912	0.6900	VVW
221	0.3207	0.3194	MW	042[b]	0.7214	0.7217	WM
112	0.3268	0.3259	MW	203	0.7308	0.7294	W
131	0.3600	0.3587	S	123	0.7400	0.7400	VW
301	0.3793	0.3783	SM	142	0.7574	0.7564	W
022		0.3772		051	0.7851	0.7833	VVW
230	0.3985	0.3973	MS	151	0.8188	0.8180	S
311	0.4083	0.4070	WM	402		0.8184	
122	0.4130	0.4120	W	341	0.8383	0.8376	MS
212	0.4316	0.4301	MS	223	0.8450	0.8442	M
040	0.4611	0.4593	MW	250	0.8574	0.8566	M
321	0.4948	0.4932	M	313		0.9318	
400	0.5566	0.5560	WM	422	0.9336	0.9332	S(B)
132		0.5555		501		0.9343	
141	0.5610	0.5596	MW	511	0.9634	0.9630	MS

[a]Chromium Kα mean radiation (λ = 2.29092 Å); a = 6.145; b = 6.761; c = 4.472.

[b]From this value on, the observed $\sin^2\theta$ values were resolved into their Kα1 and Kα2 components.